Drosophila Hamlet mediates epithelial tissue assembly of the reproductive system

Huazhen Wang[1], Ludivine Bertonnier-Brouty[2,3], Isabella Artner[2,3], Jiayu Wen[4,*] and Qi Dai[1,*]

1 Department of Molecular Bioscience, the Wenner-Gren Institute, Stockholm University, Sweden

2 Lund Stem Cell Center, Lund University, Lund, Sweden

3 Lund University Diabetes Center, Lund University, Malmö, Sweden

4 Division of Genome Sciences and Cancer, The John Curtin School of Medical Research, The Australian National University, and Australian Research Council Centre of Excellence for the Mathematical Analysis of Cellular Systems.

[*] Co-corresponding authors

Abstract

Epithelial tissue fusion requires coordinated molecular events at the ends of two epithelial structures. Regulatory mechanisms controlling these events remain largely elusive. In the *Drosophila* reproductive system (RS), this fusion unites the gonad and the genital disc-derived tissues, into a continuous tube. This study unveils the pivotal role of Hamlet (Ham), a *Drosophila* PR-domain containing transcription factor, in orchestrating epithelial tissue fusion in the RS. Loss of *ham* leads to sterility and disconnection between the testes (TE) and seminal vesicles (SV). Systematic analysis of Ham-downstream genes reveals cytoskeletal, metabolic regulators and signaling pathway components. Ham activates genes for epithelial differentiation and remodeling, while repressing genes required for tissue growth and patterning. Using multiplexed in situ hybridization, we demonstrate spatial-temporal gene expression dynamics in contacting epithelia. Key Ham downstream effectors include E-Cadherin (E-Cad), Toll (Tl) and Wnt2 signaling pathways, regulating tissue interaction and fusion. Our findings present a comprehensive gene network crucial for heterotypic epithelial tissue fusion. Mammalian Ham orthologs PRDM3 and PRDM16 are highly expressed in epithelial tissues, suggesting a conserved role across species.

Introduction

Epithelial tissue fusion is a crucial process for building epithelial tubular network and uniting separate ends [1, 2]. Studies from different model systems, like neural tube fusion and *Drosophila* tracheal development, have provided several mechanistic insights into epithelial fusion process. For instance, specialized cells at the leading edge migrate and interact using cytoskeleton protrusions [3-9] and small GTPases like Rac and Cdc42 [10]. Upon contact, the leading cells re-establish polarity and connections with the help of extracellular matrix molecules, apical proteins and E-Cad [11]. However, the exact regulators and mechanisms controlling epithelial fusion remain to be determined, especially in a context-specific manner.

The reproductive system in animals comprises tissues from different origins, and must unite to form a connected system for producing and delivering gametes. For example, the human testis is directly linked to a complex tubular system consisting of the efferent and epididymal ducts [12]. Anomalies in the fusion of these ducts are a significant cause of cryptorchidism, affecting at least three percent of newborn boys. However, there is little understanding of the molecular mechanisms guiding the patterning and fusion of these ducts.

Similarly, the *Drosophila* male RS (**Fig. 1A**) includes the gonad-derived testis and the genital disc (GD)-formed seminal vesicle, accessory gland (AG), ejaculatory duct (EJD) and additional supportive structures. During development, the TE and SV grow toward each other and merge into a continues tubular system [13]. This involves two epithelial ends, the terminal epithelial cells in the testis and the SV epithelium. Thus, the developing *Drosophila* RS provides a representative *in vivo* context to dissect mechanisms underlying epithelial tissue assembly.

Ham belongs to the PR domain containing protein (PRDM) family whose members are evolutionarily conserved cell fate regulators [14, 15]. The PRDM proteins are characterized by the presence of an N-terminal PR (PRDI-BF1 and RIZ1 homology) domain which is similar to the catalytic SET domain shared by histone methyltransferases. Dysfunction of the human orthologs of Ham, PRDM16 (Mel1) and PRDM3 (Evi1, MECOM), has been found in a variety of human abnormalities including congenital diseases, metabolic disorders and cancers [16-23]. Moreover, in at least two types of epithelial cancers (kidney and pancreas cancers), PRDM16 was shown to play a tumor suppressive role [20, 23], indicating its importance in

maintaining epithelial integrity. However, it remains undermined how these PR factors regulate epithelial tissue development and homeostasis.

Ham was exclusively studied in the nervous system where it is required for neuronal dendrite morphogenesis [24] and cell fate maintenance [25-27]. Ham was shown to repress gene expression through modulating chromatin states [28] or interacting with the co-repressor CtBP [25, 28]. However, the molecular functions of PRDM16 and PRDM3 are versatile, with their PR domains possessing intrinsic histone methyltransferase activity [17, 29] and the ability to interact with various co-activators and co-repressors [14, 30]. It remains unknown whether Ham plays a role outside of the nervous system and whether Ham also has dual function in gene expression.

In this study, we discovered that Ham is a master regulator in guiding epithelial tissue patterning and fusion in the *Drosophila* RS. Even a slight reduction of Ham disrupts epithelial differentiation and tissue assembly in the RS, ultimately affecting sperm and egg delivery. To explore new mechanisms governing epithelial tissue fusion in the RS, we conducted systematic analyses using RNA-sequencing (RNA-seq), Cleavage Under Targets and Tagmentation (CUT&TAG), multiplexed in situ hybridization data and genetic screening. These analyses led to identification of gene regulatory networks required for epithelial tissue fusion. Ham activates a gene network to promote epithelial cell differentiation and remodeling while suppressing another gene network involved in cell specification and early patterning. These target genes exhibit spatial-temporal expression dynamics during the fusion of the TE and SV. As a key Ham downstream effector, Wnt2 signaling regulates epithelial cell communication and interaction. By elucidating the regulatory network controlled by Ham, our study provides novel insights into the molecular mechanisms underlying epithelial tissue fusion.

Results

Drosophila RS development is vulnerable to reduced Ham activity

While PRDM16 and MECOM are critical cell fate regulators in various developmental contexts in mammals, the genetic roles of Ham were mainly found in the central and periphery nervous systems [24-27]. To systematically study Ham function, we generated new frameshift alleles using CRISPR/Cas9. The sgRNA targets the third exon shared by the three long isoforms B, D and G (**Supplementary Fig. 1A**), producing new alleles specifically disrupting the three PR-domain containing isoforms. We therefore named them $ham^{PR\Delta}$. The original ham^{1} and the null allele ham^{SK1} shifted open reading frame (ORF) for all predicted isoforms [24, 26].

We validated nucleotide deletions in the new alleles by sanger sequencing (**Supplementary Fig. 1B**) and protein deletion by western-blot using an antibody against Ham. The Ham antibody detected several bands in the blot (**Supplementary Fig. 1C**). The two bands at and above the 150KD marker position in the two heterozygotic controls were not detectable in the ham^{SK1} homozygous mutant, suggesting that these two bands correspond to the longest and the second longest isoforms respectively. The $ham^{PR\Delta}$ homozygous samples lack the largest band, verifying the depletion of the longest isoforms. We used one of them (-5nt) for all the later experiments.

We compared viability and sensory organ development of these alleles. In contrast to the original report showing that *ham* mutant animals died at the larval stage [24], we found that ham^{SK1}, $ham^{PR\Delta}$ and ham^{1} alleles all survived to hatch when combined in trans with the *ham* deficiency line (Df) which deletes the entire *ham* locus (**Supplementary Fig. 1D**). While ham^{1}/Df and ham^{SK1}/Df animals all died right after hatching, about two thirds of the $ham^{PR\Delta}$/Df mutants were viable without obvious gross defects. Furthermore, Ham is known to specify internal cell types (the neuron and sheath) in the mechano-sensory organ lineage, as ham^{1} mutants exhibited ectopic external cell types (the socket and shaft) with the expense of internal cells [25]. $ham^{PR\Delta}$ mutants displayed normal sensory bristles, in contrast to defective sensory organs in the ham^{1} and ham^{SK1} alleles (**Supplementary Fig. 1E**). Thus, the PR-containing isoforms of Ham are dispensable for mechano-sensory organ development and viability.

However, *ham*$^{PR\Delta}$ mutant animals showed abnormal RS morphology (**Fig. 1B**) and impaired fertility in both male and female animals (**Fig. 1C, Supplementary 2A-B**). The TE, AG and SV structures were disrupted in males, while mature eggs were stuck in the mutant female ovaries, indicating failed egg delivery. To confirm that the defects are induced by the *ham* mutation, we performed a rescue experiment by utilizing a pBAC transgene that carries the genomic region of *ham* with the super-folding GFP (sfGFP*)* coding sequence in frame with the *ham* ORF. The pBAC transgene rescued the viability of all *ham* mutant conditions, and at least partly restored their male fertility (**Fig. 1C**). Together, these results indicate that the *ham*$^{PR\Delta}$ allele represents a hypomorphic condition which preserves Ham shorter isoforms and partial activity. Thus, although viability and sensory organ development do not require the PR-containing isoforms, formation of the RS depends on them.

Ham-expressing epithelial cells connect the gonadal and supportive tissues

To assess how Ham controls RS development, we examined Ham expression in the developing RS using a V5 antibody which detects all Ham isoforms in the *ham_V5* allele [31]. Ham_V5 was detected in the connecting tube of the adult SV and TE (**Fig. 1D**), suggesting a direct involvement of Ham in regulating RS formation.

During RS development, the TE terminal epithelial cells are specified in the embryo as male-specific somatic gonadal precursors (msSGPs) [32]. The SV epithelium, together with AG, develops from a group of mesenchymal cells in the GD which undergo mesenchymal-to-epithelial transition (MET) during the larval stage (**Fig. 1E**) [33, 34]. Notably, in the L3 larval male RS, Ham_V5 was detected in the TE terminal epithelial cells as well as the btl-Gal4-expressing mesenchymal cells in the GD (**Fig. 1F**).

In the pupal RS, multiple events, including epithelial tube formation and fusion as well as myoblast and pigment cell migration, are tightly coordinated (**Fig. 1G**) [35]. At this stage, a high level of Ham persists in the TE terminal epithelial cells, SV and AG (**Fig. 1H-J**). In contrast, Ham is barely detectable in the SV myoblasts/myotubes labeled by the reporter, mef2-Gal4-driving UAS-GFP (**Fig. 1J**). Similarly, high levels of Ham_V5 were found at the joint sites of female oviducts and ovaries during both pupal and adult stages (**Supplementary Fig**

2C). Thus, Ham is an intrinsic factor in epithelial cells at the connection site between the gonadal- and genital-disc derived tissues in both males and females.

Ham is required for epithelial tissue fusion in the developing male RS

The specific expression of Ham and mutant phenotypes in the RS prompted us to investigate its function in RS epithelial tissues. Here we focused on the male, as the assembly of the TE and SV represents a remarkable process involving a series of tissue reorganization events (**Fig. 1G**). When the two ends of TE and SV get close, the epithelial cells at the leading edges meet and form a common epithelial tube. In the meanwhile, myoblasts from the SV and pigment cells from the TE migrate toward the opposite direction. Myoblasts further differentiate into myotubes, forming a thin layer of muscular sheet and sculpting the TE into a "spirals" shape [36].

We found that at 40-50h APF the TE and SV tubes in $ham^{PR\Delta}$*/Df and hamSK1/Df* mutants did not properly elongate and appeared shorter and wider compared to that in the wild-type (**Fig. 2A**). The mutant TE appeared as a sphere shape, indicating failed myotube migration. The SV and AG were only partly elongated in the $ham^{PR\Delta}$ mutant, and even unseparated in the *ham* null allele *hamSK1/Df*. This suggests that the severity of RS abnormality correlates with the levels of reduction in *ham* gene products.

To examine epithelial integrity, we performed immunofluorescent staining using the antibodies against the epithelial cell markers, E-Cad (adherent junctions) and Coracle (Cor, septate junctions equivalent to mammalian tight junction) protein. We also incorporated an SV-specific transgenic reporter, btlGal4-driving UAS-EGFP or UAS-CD8GFP, to the control and *ham* mutant genotypes. E-Cad is enriched at the apical side (the lumen side, **Fig. 2B**) of the TE and SV epithelial tubes. Notably, the TE terminal epithelium accumulates a higher level of E-Cad compared to the SV epithelium, while Cor is mainly expressed at the SV side but not much in the TE, suggesting a heterotypic nature of the TE terminal and SV epithelia.

Control animals always showed connected TE and SV, whereas ham mutant TE and SV tissues were either separated from each other, or appeared contacted but only with disconnected epithelial tubes (**Fig. 2B, Supplementary Fig. 3A**). Importantly, this phenotype can be fully

rescued by the *pBAC_ham_sfGFP* transgene, confirming that it is caused by the *ham* mutation. These observations suggest that the epithelial ends of the TE and SV possess distinct properties despite both being epithelial cell types and that Ham is required for TE and SV fusion.

Depletion of Ham abolishes TE terminal epithelial cell formation

A close inspection on the pupal TE revealed that most of TE epithelial cells were missing in *ham* mutant animals (**Fig. 2B, Supplementary Fig. 3A**). *ham* mutant lava also either lacked TE epithelial cells or showed abnormal location of these cells, which can be rescued by the *pBAC_ham_sfGFP* transgene (**Supplementary Fig. 4A**). TE terminal epithelial cells derive from male specific gonadal precursors (msSGPs) specified in the early embryo (**Supplementary Fig. 4B**) [33] and expand during larval and early pupal stages. This result indicates that Ham regulates specification or survival of these cells. Indeed, we detected Ham expression in msSGPs and other SGPs in the embryonic gonad. The number of msSGPs labeled by Abd-B or Sox100B-GFP was dramatically reduced in S13 and S15 *ham* mutant embryo (**Supplementary Fig. 4C-G**). Our data suggest Ham to be a master regulator for the specification and/ or survival of msSGPs, and the absence of msSGPs accounts for loss of TE terminal epithelial cells in larval and pupal stages.

Ham regulates patterning and cell differentiation of the RS epithelial tubes

The epithelial cells in the SV and AG originate from a group of mesenchymal cells recruited by the FGF pathway involving Btl and Branchless (Bnl) [33, 34]. These cells undergo MET to form an epithelial mass which then cavitates to generate inner hollow space and eventually elongates into an epithelial tube. In comparison with the control, the signal intensity of both E-Cad and Crumbs (Crb) were significantly reduced in *ham* mutant SV epithelial cells, which coincides with the shortening of septate junctions labeled by Cor (**Fig. 2C-E**). This result suggests that Ham regulates epithelial cell differentiation in the SV. To check whether Ham regulates epithelial cell differentiation in the TE, we used the FRT/FLP system (see Methods) to generate mosaic somatic mutant clones. In these animals, *ham* mutant cells were GFP negative, while wild-type and *ham* heterozygous cells expressed GFP (**Fig. 2F, Supplementary Fig. 3B**). The E-Cad levels at the border between two mutant cells were significantly lower than those between wild-type cells, indicating that *ham* depletion impaired differentiation of TE terminal epithelial cells.

In summary, these phenotypic analyses suggest that Ham controls formation of TE terminal epithelial cells in the early embryo and regulates epithelial tube elongation and cell differentiation at the pupal stage. Thus, failed epithelium fusion in *ham* mutant RS could result from: 1) absence of TE terminal epithelial cells, 2) defects in epithelial tube elongation and cell differentiation of the SV and 3) a combination of both.

Ham directly controls epithelial fusion between the TE and SV

Next, we sought to assess whether and how Ham directly regulates the fusion process. We first attempted to generate a mild mutant condition which can bypass defects of TE epithelial cell loss and SV-AG tube elongation. We chose RNAi knockdown because knockdown efficiency can be enhanced by overexpressing Dicer2 (Dcr2) and modulated by temperature when RNAi is controlled by the GAL4/UAS system.

We first identified a Gal4 driver expressed in the SV and AG epithelial cells, after screening the available Gal4 transgenes driven by a series of genomic fragments spanning the *ham* locus [37] (**Supplementary Fig. 5A**). This transgene (thereafter named as *hamRSGAL4*) induces high expression of *UAS-GFP* in the TE and SV epithelial cells and a weak expression in the myoblasts (**Supplementary Fig. 5B**). Myotubes appeared at the junction site of the TE and SV and could migrate to the surface of the testis in the *ham* mutant (**Supplementary Fig. 5C-D**), confirming that loss of *ham* does not abolishes myoblast fusion or myotube migration. *hamRSGAL4*, when driving a *ham* RNAi line, nearly abolished Ham expression in animals carrying the *UAS-dcr2* transgene (**Fig. 2G-H,** the middle panels). These animals also had a reduced number of TE epithelial cells and displayed a ball-like structure of the GD, similar to the *ham* null allele. Without *UAS-dcr2*, *ham* RNAi knockdown reduced Ham expression but preserved TE epithelial cells and normal-appearing SV. Remarkably, the TE and SV epithelia still failed to fuse (**Fig. 2H,** the right panel), suggesting that Ham also controls the late step of fusion. Furthermore, E-Cad staining intensity was significantly reduced in *ham* RNAi TE but not in *ham* RNAi SV (**Fig. 2I-J, Supplementary 3C-D**), suggesting that expression of E-Cad in the TE is sensitive to even mild reduction of Ham protein levels.

Ham controls distinct molecular pathways to promote tissue assembly.

To identify mechanisms that control epithelial fusion, we started to investigate Ham downstream target gene network. We performed RNA-seq experiments from dissected TE and SV tissues during the stage of 18-25h APF. We used two pairs of genotypes, including the wild-type (*wt*), and $ham^{PR\Delta}$ homozygous and the *wt/Df* and *hamSK1/Df* trans-heterozygous (**Fig. 3A**). The comparison between the first pair will determine dysregulated genes in the $ham^{PR\Delta}$ hypomorphic condition, while the comparison between the second pair will identify genes that change expression between the null and *ham* heterozygous conditions.

The principal component analyses validated consistency between the three biological replicates (**Supplementary Fig. 6A**). To not exclude small gene expression changes (*e.g.* in the leading cells which are the minority within the whole tissue), we used a loose cutoff (FDR < 10% and FC>1). We found more than two thousand up-regulated and down-regulated genes in the GD. In the mutant TE, there were similar numbers of dysregulated genes (**Fig. 3B**). The genes that only changed expression in one condition could result from unspecific genetic background, differential dependence on the PR-containing isoforms or different sensitivity to *ham* heterozygous condition.

Expression of many dysregulated genes can be indirectly affected by Ham. We next intended to identify genes that are transcriptionally regulated by Ham. To this end, we determined Ham genomic binding sites using Cleavage Under Targets and Tagmentation assays (CUT&TAG) [38] on finely-dissected TE and grossly-dissected abdominal tissues in which Ham is mainly expressed in the TE and SV epithelium (**Fig. 3A**). We used a Ham antibody for wildtype tissues, a GFP antibody for tissues from the *pBAC_ham_SFGFP* transgene and IgG as a negative control in parallel for all the samples. Using the SEACR software, we identified peaks and intersections of peaks across the Ham and GFP antibody conditions (see Methods). We performed principal component analyses and found the GFP antibody gave more consistent peak calling from replicates (**Supplementary Fig. 6B**). For subsequent analyses, only the common 3433 and 691 peaks identified by the two antibodies (Ham and GFP) were included to ensure signal specificity (**Fig. 3C-D**).

To determine Ham target genes, we intersected the RNA-seq data from the hamSK1/Df versus wt/Df comparison with the Cut&Tag data. Among the 2,546 up-regulated genes in the GD, 441 (17.3%) contained Ham CUT&TAG peaks. Among the 2379 downregulated genes, 569

(23.9%) showed Ham binding (**Fig. 3E**). In the TE, a lower fraction of dysregulated genes contains Ham CUT&TAG peaks, including 4.7% (108/2274) upregulated genes and 7% (144/2057) downregulated genes (**Fig. 3F**), suggesting that dysregulated genes in the mutant TE are mainly indirectly controlled by Ham.

Both up- and down-regulated genes contain Ham binding peaks, suggesting that Ham can repress and activate gene expression. To systematically explore the function of Ham-regulated genes, we performed gene network analysis using STRING [39]. We focused on the genes bound by Ham and also dysregulated in the genital disc (GD) in the null condition *hamSK1*, considering that most of TE genes are only indirectly influenced in the ham^{SK1} mutant. The SRING MSL clustering analysis generated 114 functional clusters from down-regulated genes and 62 clusters from up-regulated genes (**Fig. 4A, Supplementary Table 1**). Interestingly, many of downregulated genes clustered into several large groups including cytoskeleton regulators, metabolic factors, cell adhesion and extracellular matrix proteins, suggesting that Ham activates genes to promote epithelial differentiation and remodeling. In contrast, upregulated genes are enriched for patterning factors, cell cycle genes and transcriptional and translational regulators, suggesting that Ham suppresses early developmental processes. Notably, metabolic factors are enriched in both categories, but these factors belong to distinct functional groups. Thus, epithelial fusion requires complex and balanced metabolic processes. Together, this network analysis confirms that Ham positions on top of distinct molecular pathways to facilitate TE and SV assembly.

Ham was known for its repressive activity via interacting with the co-repressor CtBP and influencing histone modifications [28]. Our finding of its activation function was unexpected. To validate the activation activity of Ham, we chose three downregulated target genes (**Fig. 4B**), *dwnt2*, *shot* and *shg*, for transcriptional reporter assays. *shg* encodes E-cad, while Shot is a member of the spectraplakin family of large cytoskeletal linker molecules simultaneously binding to actin and microtubules. The function of *wnt2* was reported in the developing RS development [40, 41]. We cloned four genomic fragments from the *wnt2* locus, two each from *shg* and *shot* into a luciferase construct, and co-transfected each reporter with individual plasmids expressing several variants of Ham. In addition to the Ham long isoform and a PR truncation version of Ham, we included the NZF and the CZF domains fused with the VP16 activation domain (NZF_VP16 and CZF_VP16) (**Fig. 4C**). The two ZF domains of Ham are putative DNA binding domains, but it remained undetermined whether they help to recruit Ham

to DNA. This experimental setting allows to assess which of the ZF domains is able to target Ham-regulated enhancers. The full-length, the PR truncation and the NZF_VP16 fusion all activated expression of the reporters driven by 7 out of 8 Ham-bound elements (**Fig. 4D-G, Supplementary Fig. 6C-D**). By contrast, the CZF_VP16 had little activity on the reporters. This result confirms that Ham can directly activate target gene expression and that the NZF domain directly or indirectly recruits Ham to enhancers.

To further identify co-factors with which Ham interacts to regulate gene expression, we performed *de novo* motif discovery from Ham CUT&TAG peaks in mixed TE and GD tissues close to up-regulated and down-regulated genes in the *hamSK1* mutant using the MEME-ChIP software. This resulted in nine and five significantly enriched motifs from up- and down-regulated gene loci respectively (**Supplementary Fig. 6E**). While five motifs were shared between these two sets, the motifs for Dpp/BMP signaling factor MAD, the zinc-finger protein ZNF263 and two unknown factors were only enriched in the upregulated genes. The result implies that Ham may switch activation to repression activity when interacting with these co-factors in the context of RS development.

Ham downstream effector genes are required for male RS fertility.

Built upon our transcriptomic data, we next intended to identify genes crucial for the fusion process. We reasoned that as the majority of TE terminal epithelial cells are lost in both *ham* mutant alleles, the commonly downregulated genes in $ham^{PR\Delta}$ and ham^{SK1} TE (**Fig. 3B**) may be expressed in the *wt* TE epithelial cells and can be functionally important. We thus focused on the top 241 common downregulated genes whose expression showed a fold change greater than 1.5, and the three validated Ham target genes: *shot*, *wnt2* and *shg*. Using all available RNAi lines from the Bloomington stock center that cover 113 out of 244 candidate genes, we performed a UAS-RNAi screen with the *UAS-dcr2*; *hamRSGal4* driver for male fertility (see Methods).

The RNAi screen led to identification of 26 genes whose knockdown abolished or reduced male fertility (**Supplementary Table 2**). Knocking down four of these genes, *shg*, *AP2-alpha*, *pebble (pbl)* and *CG11406*, resulted in complete sterility, indicating their importance for male fertility. We defined this category as 100% penetrance of sterility. Knockdown of other twenty-

two genes reduced fertility to different extent (**Fig. 5A-B**). Given that the *hamRSGal4* driver is highly expressed in the TE and SV epithelia, we expect highly effective knockdown occurs only in these epithelial cells. However, *hamRSGal4* also drives a weak expression in the myoblasts before they differentiated into myotubes (**Supplementary Fig. 5B)**, which may result in a non-tissue autonomous effect when knocking down the candidate genes expressed in myoblasts.

Consistent with the gene network analysis (**Fig. 4A**), these genes include cytoskeleton regulators (*pbl*, *shg*, *shark*) [42-44] and metabolism factors (*CG11406, Ph4alphaMP, GstE11, CG17477, CG11069, AdSL, CG17283, CG15117, CG7484*). Other genes are known or predicted to be involved in intracellular membrane trafficking (*AP-2alpha*, *CG31935* and *CG7456*) [45] and signaling (*wnt2*, *Toll*, *AkhR*, *Idgf4* and *Hr46*) [46-49].

We confirmed that knocking down *pbl*, *AP-2alpha*, *CG11406* and *shg* led to failed TE and SV fusion and abnormal morphology at the pupal stage (**Fig. 5C, Supplementary Fig. 7-8)**. *pbl* encodes a Rho guanine nucleotide exchange factor, implicated in multiple processes involving cytoskeleton reorganization[42, 50, 51]. The gene product of CG11406 is a predicted triglyceride lipase, cleaving triacylglycerol (TAG) to produce diacylglycerol (DAG). AP-2alpha, a subunit in the Adaptor complex 2, is involved in intracellular trafficking and secretion [52]. Remarkably, *shg* knockdown also led to aberrant mobilization of TE epithelial cells to the middle of the TE, while no such effect was found in the SV and AG. Downregulation of E-Cad is a key event during epithelial to mesenchymal transition (EMT), and E-Cad promotes cohesive cell migration of mesenchymal cells, but suppressing cell motility of epithelial cells [53, 54]. Our result suggests that the SV and the TE terminal epithelia have distinct dependence on E-Cad and that TE epithelial cells are prone to becoming motile when E-Cad is reduced. Together, this screen identified a collection of known and novel factors involved in epithelial tissue fusion, confirming that the fusion process requires coordinated activity of several classes of molecules.

Ham downstream genes exhibit spatial- temporal expression dynamics in the male RS

During epithelial fusion, cells at the leading edge become specialized and express specific genes required for tissue interaction and remodeling [1, 2]. Moreover, as we observed, the TE

terminal and SV epithelia have distinct properties, suggesting that these two sets of epithelial cells may express distinct genes. We thus intended to assess spatial distribution of Ham downstream genes. We conducted a high-resolution multiplexed RNA *in situ* hybridization assay known as SCRINSHOT (single cell RNA *in situ* hybridization on tissues) [55] to visualize expression of candidate genes. These genes include *wnt2*, *shg* and *shot* as these genes were either known for male RS development (*wnt2 [40]*) or epithelial tissue fusion (*shg* [56] and *shot [57]*), and the positive genes from the RNAi screen, along with the receptor genes in Wnt2 signaling (*fz*, *fz2*, *fz3* and *fz4*) and ligand genes in Tl-signaling (*spz*, *spz4*, *spz5* and *spz6*) (**Supplementary Table 3**). Some of these Wnt2 and Tl signaling genes displayed dysregulation in at least one of the *ham* mutant alleles according RNA-seq data (**Supplementary Fig 9A-B**). Other receptor genes in Wnt signaling and ligand genes in Tl signaling were omitted due to low read numbers in the RNA-seq data, indicating negligible or minimal expression in the TE and GD.

Each SCRINSHOT reaction took place within a mini-chamber, accommodating pairs of control and *ham* mutant tissues, or GFP KD control and ham RNAi KD samples (refer to Methods for details of probe design and experimental procedures). This setup was designed to minimize technical variability between the genotypes. mRNAs are visualized as fluorescent dots in SCRINSHOT images, with each dot representing a single mRNA molecule. However, due to the densely packed nature of cells in the TE and SV tissues, quantifying mRNA molecules at a single-cell resolution is challenging. Therefore, we opted to quantify fluorescent signal intensity within defined areas (see Methods). In total, 37 genes were tested, including *ham* itself (**Supplementary Table 3**). Probes for 7 genes gave either no or low signal in the TE or GD, likely attributed to poor probe quality, given their RNA-seq read numbers not being low. Resembling Ham protein expression (**Fig. 1F**), *ham* mRNAs were detected in the TE terminal epithelium (**Fig. 6A, Supplementary Fig. 10A**), confirming the specificity of the SCRINSHOT method. Similarly, *wnt2*, *shg* and *shot* all exhibited high expression in the TE terminal epithelium (**Fig. 6A, Supplementary Fig. 10A**).

In total, 25 genes exhibited detectable SCRINSHOT signal in the wt SV and AG, while 29 displayed signals in the wt TE (**Supplementary Table 3)**. Within the TE, 17 out of 29 were specifically localized in the TE terminal epithelial cells, with the remaining 12 detected only in other TE cells (**Fig. 6A, Supplementary Fig. 10-13, Supplementary Table 3**).

Subsequently, our analysis focused on the genes expressed in the TE terminal and SV epithelia. While 17 genes exhibited expression in both epithelial ends (**Fig. 6A-B, Supplementary Fig. 10A-B**), 8 were exclusively expressed in SV epithelial cells (**Fig. 6F**, **Supplementary Table 3**), underscoring the heterotypic nature of the TE and SV epitheliums. Notably, certain genes (CG11406, *AP-2alpha*, *GstE11*, *Tl*, *spz5* and *spz6*) demonstrated temporal dynamic expression in the TE epithelium: spz5 and CG11406 are present during the 20-25h APF timeframe, prior to fusion, but gone during the 28-32h APF period when the TE and SV are undergoing fusion; *AP-2alpha*, *GstE11*, *Tl* and *spz6* showed the opposite trend, being expressed only later (**Fig. 6, Supplementary Fig. 10-12**).

In the GD, while the majority of genes exhibited ubiquitous expression, *wnt2* and *spz* were predominantly expressed in the leading cells within the SV, contrasting with their expression in the remaining GD (**Fig. 6B**). Additionally, the expression patterns of *fz2*, *fz3* and *Tl* displayed spatial specificity: fz2 exhibited higher expression levels in the SV compared to the AG, *fz3* demonstrated the opposite pattern with higher expression in the AG, and *Tl* was primarily expressed in the myoblasts (**Fig. 6B**). These findings imply that Wnt2 and Tl signaling may have cell-type-specific roles in the fusion process. Thus, SCRINSHOT mapped 30 candidate genes in the developing GD and TE, with 29 of them display spatial or temporal dynamics.

Wnt2 and Tl signaling pathways are key mediators of Ham function in RS tissue assembly

Next, we aimed to identify genes exhibiting altered expression in *ham* mutant SV and TE. As *hamSK1* mutant TE lacks terminal epithelial cells, we excluded TE samples and only quantified SCRINSHOT signal levels in the developing SV between *wt* and the *hamSK1* mutant. In contrast, *ham* RNAi knockdown resulted in fusion defects but only mildly impacted SV morphology and TE terminal epithelial cell number (**Fig. 2G-H**). These samples allow to assess gene expression alterations in both the SV and TE epithelia.

ham fluorescent intensity appeared comparable between *wt* and mutant samples (**Fig. 6B, D-E, Supplementary Fig. 10-13**), suggesting that *ham* mutant RNAs, containing the CRISPR-generated indels, remain stable at this stage. In the *hamSK1* mutant SV, seven genes became downregulated, while two exhibited upregulation. The downregulated genes were four Wnt2 pathway genes (*wnt2*, *fz*, *fz2*, *fz4*), one Tl pathway gene (*spz*), and *shg* (**Fig. 6B-**C, **Supplementary Fig. 10**). Notably, *wnt2*, *fz*, *spz* and *shg* also displayed downregulation in *ham*

RNAi SV (**Fig. 6D-E, Supplementary Fig. 10**), suggesting that these genes and their associated signaling pathways may be directly involved in the fusion process downstream of Ham. The upregulated genes in *hamSK1* mutant SV include *GstE11* and *CG11069* (**Supplementary Fig.11C, E**), which exhibited low expression in the leading cells of wt SV epithelium, but increased expression under the *hamSK1* condition. In *ham* RNAi knockdown animals, *CG11069* was again upregulated, while *GstE11* did not change expression. Instead, another ligand gene in Tl signaling (*spz5*) displayed increased expression (**Supplementary Fig.11D, F**). On the TE side, only four genes showed expression alteration in *ham* RNAi animals, including *ham* itself, *shg*, *fz* and *fz2* **Supplementary Fig.11G**), implicating functional requirement of these genes in both TE and SV epithelia.

The observation that knocking down *Tl* resulted in decreased male fertility (**Fig. 5B**, **Supplementary Table 2**), coupled with the expression of multiple *spz* ligand genes in the developing TE and SV, suggests that the Tl signaling pathway might be required for assembling the TE and SV. To investigate this possibility, we examined male flies with *spz* knockdown driven by *hamRSGal4*. These animals produced a comparable number of progenies to control animals. The lack of phenotype in this condition could be attributed to inefficient knockdown or genetic compensation by another *spz* gene, like *spz5* whose expression increased in *ham* RNAi animals when *spz* expression was reduced. In addition to Tl, two other Tl related genes (Toll-7 and Toll-9) exhibited moderate number of reads in the RNA-seq data. We then tested male fertility in *Toll-7* and *Toll-9* knockdown animals. *Toll-9* knockdown led to a drastic reduction in progeny numbers compared to the RNAi control (**Supplementary Fig. 14A**). Consistent with the sterility, some of the *Toll-9* knockdown males displayed abnormal TE shape (**Supplementary Fig. 14B**). Remarkably the majority of Toll-9 knockdown animals showed empty SV without sperms (**Supplementary Fig. 14C**), suggesting failed connection between the TE and SV. Together, these results pinpoint an essential role of Tl signaling in male RS development.

To validate the role of Wnt2 signaling in RS development, we investigated four genetic conditions, aimed at modulating its level and activity: $wnt2^{O}$ (a *wnt2* null allele), *wnt2* overexpression driven by *hamRSGal4*, *fz* and *fz2* RNAi knockdown driven by *hamRSGal4*. The $wnt2^{O}$ mutant TE and GD never connect, suggesting that Wnt2 is essential for the fusion process. The $wnt2^{O}$ mutant TE lacks the pigment cell and myocyte layers (**Fig. 7A**), consistent with its reported function in these two cell types [35, 40]. The $wnt2^{O}$ mutant GD failed to form

elongated SV and AG, suggesting that Wnt2 is required for GD patterning and differentiation. Moreover, overexpression of *wnt2* also resulted in fusion defects and mis-localization of TE epithelial cells (**Fig. 7B**), a phenotype reminiscent of *shg* knockdown animals. Indeed, *wnt2*-overexpressing cells displayed reduced levels of E-Cad, suggesting that Wnt2 signaling might balance E-Cad levels to maintain TE epithelial cell properties. Consistently, *fz2* knockdown animals exhibited comparable phenotypes, including mobilized TE epithelial cells and failed tissue fusion (**Fig. 7C**). *fz2* and *fz* knockdown also decreased male fertility (**Fig. 7D**). Collectively, these results suggest the importance of optimal Wnt2 signaling levels in male RS development and epithelial tissue fusion.

Discussion

In this study we demonstrate that the transcription factor Ham plays a crucial role in controlling epithelial fusion during *Drosophila* RS development. Early in embryonic development, Ham determines the cell fate of msSGPs, which are progenitor cells for TE terminal epithelial cells. Later on, Ham directly regulates the differentiation of epithelial cells in both the TE and SV by orchestrating a gene expression program in epithelial cells. While our primary focus is on male RS, we found that Ham is also expressed in cells at the fusion site of the oviduct and ovary. Mutant females lacking functional Ham exhibit a non-functional oviduct epithelial tube, suggesting that Ham likely employs a similar mechanism to control epithelium fusion in females.

By examining *ham* mutant phenotypes and its downstream target genes, we identified several classes of novel factors involved in fusion process of SV and TE. These genes, directly or indirectly controlled by Ham, encompass a diverse array of molecular functions. This discovery provides a comprehensive gene network for future investigation of epithelial fusion processes. The cell-type-specific and tissue-specific spatial distribution of these genes suggest that they may regulate various aspects of fusion, including cell migration, intercellular communication between myoblasts/myotubes and epithelial cells, specification of the leading cells, and other steps in the fusion process. For instance, Tl and its related receptors is known to mediate cell adhesions [58]. We can speculate that Tl signaling and the molecule itself promote interaction between myoblasts and myoblasts and epithelial cells (**Fig. 7E**), based on high expression of Tl in myoblasts and the presence of multiple Spz ligands in the TE and SV epithelial cells. Moreover, *Wnt2*, *fz* and *fz2* are highly expressed in the leading cells of TE and SV epithelia, and also required for TE and SV connection, suggesting that Wnt2 signaling mediates epithelial cell communication, remodeling and fusion.

Despite being discovered more than twenty years ago [24], research on the function of Ham function has primarily focused on its roles in the nervous system. Our findings highlight a crucial function of Ham in epithelial tissues. Apart from the RS, we observed high expression of the Ham protein in other epithelial tissues including the Malpighian tubes (akin to the kidney in insects) and the intestine (data not shown). Furthermore, orthologs of Ham, PRDM16 and PRDM3/MECOM, exhibit high expression in epithelial tubular structures, such as Lung, pancreas, kidney, urinary bladder and gastrointestinal tract and lung, according to observations

in the Human Protein Atlas (**Supplementary Fig. 15**. https://www.proteinatlas.org/ENSG00000142611-PRDM16/single+cell+type; https://www.proteinatlas.org/ENSG00000085276-MECOM/single+cell+type) [59]. Notably, Seminal vesicle and ductus deferens, the equivalent structure to fly seminal vesicle, are the top one and three tissues with the highest PRDM16 expression (**Supplementary Fig. 15A**). This suggests a potential role for these proteins in controlling epithelial integrity and fusion in mammalian organogenesis. Indeed, we observed that the pancreas duct volume in mouse embryos lacking *Prdm16* is significantly reduced (data not shown). Although the exact cellular changes and the underlying molecular mechanisms in this context await further investigation, this phenotype underscores a crucial function of *Prdm16* in pancreatic epithelial duct formation.

We show that compared to Ham function in the nervous system, the PR-containing isoforms are indispensable for RS epithelial fusion and differentiation, and that Ham can directly activate epithelial gene expression. It remains to be determined whether Ham has distinct molecular functions or it regulates a subset of common molecular pathways in these two contexts. Dendrite morphogenesis involves outgrowth and branching, somewhat analogous to epithelial tube growth and branching. For instance, molecular mechanisms regulating polarized protein trafficking are crucial for both dendrite and epithelial tube branching [60]. Additionally, several transcription factors like Sequoia [61, 62], Tramtrack [63, 64] and Cut [65, 66] play roles in both dendrite morphogenesis and tracheal tube fusion. These examples suggest that there might be more unrecognized common mechanisms between dendrite and epithelial morphogenesis. It is of interest to test whether the effectors we identified in the RS epithelium are involved in dendrite morphogenesis in the nervous system.

We observed a unique aspect of epithelial fusion in the *Drosophila* RS. Unlike many epithelial fusion processes where two homologous ends merge, such as those in mammalian neural tube closure and *Drosophila* tracheal formation *etc* [1, 8, 10], the two epithelial ends in the *Drosophila* RS are heterotypic. Specifically, the TE terminal epithelial cells express higher levels of E-Cad and lower levels of Cor compared to SV epithelial cells. In response to the reduction of E-Cad or ectopic expression of *wnt2*, TE terminal epithelial cells become motile, resembling a process akin to epithelial-to-mesenchymal transition. This suggests that TE terminal epithelial cells may be more invasive during epithelial fusion. On the other hand, SV epithelial cells, despite originating from mesenchymal cells, exhibit typical epithelial cell

characteristics, including regular Cor and E-Cad expression. Notably, many genes are expressed exclusively in the SV epithelium, distinguishing it from the TE epithelium. Heterotypic epithelial fusion occurs in many developmental processes, such as digestive system formation, vertebrate optic fissure closure, and mammalian urogenital development. Failure of epithelial fusion can lead to a wide variety of developmental diseases such as oesophageal atresia, spina bifida, ocular coloboma, congenital abnormalities of the kidney, urinary tract and persistent cloaca. Studying the basic processes and key players of normal epithelial tissue fusion in an *in vivo* context will help to understand the pathogenesis of these diseases.

Acknowledgements

We thank the imaging facility (IFSU) of Stockholm University, the BEA sequencing facility at Karolinska Insitute, and the National Genomic Institute of Scilife Laboratories, Sweden, for providing service and support. The Bloomington Stock Center and the *Drosophila* community provided important reagents and fly stocks. We thank Christos Samakovlis's lab for helping to set up SCRINSHOT and Eric Lai's lab for the initial Ham reagents. Funding from Australian Research Council Centre of Excellence for the Mathematical Analysis of Cellular Systems (CE230100001) and ANU Future Scheme to J.W. The project was supported by project grant from Swedish Research Council (Vetenskapsrådet, 2020-03543) and Swedish Cancerfonden (CAN 22 2161 Pj) to Q.D.

Author contributions

Conceptualization and project design by QD, experiments conduction by HW, preliminary test in pancreas by IA and LB, computation analysis by JW. Data interpretation by HW, JW and QD. Manuscript writing by QD with input from HW and JW.

Materials and methods

Fly strain culturing and generation of transgenes

All fly stocks were maintained at 22°C. The *ham*$^{PR\Delta}$ mutants were created using CRISPR: transgenic flies carrying single guide RNA targeting the PR domain containing isoforms were crossed into the vas-Cas9 transgenic flies. Frame-shift mutations were identified by PCR and Sanger sequencing. Transgenic flies were created at BestGene, Inc.

The ham Gal4 lines and RNAi stocks were obtained from Bloomington Stock Center. Knocking down experiments were performed at 25 °C and with a regular 12-hr light–dark cycle.

To generate ham null mutant somatic clones in the TE terminal epithelium, *hamsk1 FRT40A/CTG* males were crossed with virgin females carrying the genotype *hsFLP(X); hsGFP.nls FRT40A.* Embryos aged 0-5 hours were collected and developed at 25°C until the 2nd instar larval stage. GFP-negative larvae, indicating the genotype *hsFLP(X); hsGFP.nls/hamsk1 FRT40A*, were then selected. Head shock treatments at 37°C for 1 hour were administered three times during the 2nd and 3rd instar larval stages to induce somatic clones. Prior to dissection, another 1-hour head shock at 37°C was performed to induce GFP expression, marking the wild-type cells.

Fertility test

For ham mutants, single male or female with indicated genotype was mated with two w^{1118} virgin females or two w^{1118} males on day 0 of the experiment. Crosses were flipped every 2 days for 3 consecutive times. Progenies from the second vial with eggs laid between day 2-4 were counted after 2 weeks.

For the RNAi screen, individual UAS-RNAi males were crossed with females carrying UAS-dcr2 and hamRSGal4. The resultant F1 male progenies (2-5 days old) with the genotype UAS-dcr2; hamRSGal4>UAS-RNAi were crossed to w^{1118} virgin females (1-2 days old) on day 0 of the experiment. In each test, four males were crossed with three females. Crosses were flipped on day2 and day3 for pre-laying. After flipping on day3, crosses were kept in the new vial for egg laying for a specific time period (GroupA: 48hours; GroupB: 16-18h; GroupC: 7-8h). If at

least three males and two females were alive, then the flies were transferred to a new vial, the old vial was kept, and all progenies were counted.

For fertility test of the Wnt2 and Tl signaling pathways components, UAS-RNAi males were crossed to virgin females of the genotype UAS-dcr2; hamRSGal4. Two F1 male progenies (1-2 days old) with the genotype UAS-dcr2; hamRSGal4>UAS.RNAi were crossed to three w^{1118} virgin females (1-2 days old) on day 0 of the experiment. Crosses were flipped every day for 4 consecutive times. Progenies from the fourth vial with eggs laid between day 3-4 were counted after 2 weeks.

Immunostaining

For embryo staining: embryos were collected, dechorionated with bleach and fixed with 4% formaldehyde in PEM (0.1M PIPES, 2mM EGTA, 1 mM MgSO4, pH 7) for 20 min. For immunostaining, embryos were rehydrated, washed with PBT (0.3% Triton X-100 in PBS) and blocked with PBSBT (0.3% Triton X-100, 1% BSA in PBS).

For tissue staining: tissues were dissected from stage defined larvae or pupae in 1xPBS within 30 min and fixed in 4% paraformaldehyde in PBS for 20min. For immunostaining, dissected tissues were washed with PBT (0.1% Triton X-100 in PBS) and blocked with PBSBT (0.1% Triton X-100, 1% BSA in PBS).

For both embryo and tissue staining, the primary antibodies were diluted with PBSBT (0.1% Triton X-100, 1% BSA in PBS) and incubated at 4°C over night. After extensive washing with PBSBT (15min x 4 times), the secondary antibodies were added in 1:500 dilution and incubated at room temperature for 2h. After washing with PBT (0.1% Triton X-100 in PBS), the samples were counter-stained with DAPI and mounted in Vectashield (Vector Laboratories).

The following primary antibodies were used: Rabbit anti-Ham (1:300) (Gift from Eric Lai's lab), Ms anti-V5 (1:500, R960-25, invitrogen), chk anti-GFP (1:2000, ab13970, Abcam), Rat anti-vasa (1:50, anti-vasa-c, Developmental Studies Hybridoma Bank, DSHB), Ms anti-ABD-B (1:50, 1A2E9-c), Ms anti-SXL (1:50, M18-c), rat anti-DE-Cad (1:50, DCAD2, DSHB), mouse anti-Crb (1:10, Cq4 DSHB), mouse anti-Coracle (1:100, C615.16 DSHB). Secondary antibodies conjugated to Cy3 or Cy5 or Alexa Fluor-488 (Jackson ImmunoResearch) were used.

Quantification of signal intensity from fluorescent immunostaining

For E-Cad and Crb in Figure 2, "raw intensity density" from manually defined regions (using free-hand drawing) along the apical side of the SV and TE terminal epitheliums was obtained in ImageJ. For each sample, 2 regions in the SV and 3 regions in the TE terminal epithelium were averaged. The regions used to determine relative E-Cad fluorescence in *hamSK1* TE somatic clones were at the apical side between cell junction. The length of Cor-stained cell junction was measured using ImageJ. A straight line was drawn over the Cor staining with the 'Freehand Line tool'. For each sample, the average length from 10 cell-cell junctions were used. In all experiments, images for the genotypes in comparison were always processed using exact settings. At least three biological replicates were included in statistical analysis.

Western Blot

Embryos from *w1118*, $ham^{PR\Delta}$*/CTG*, ham^{SK1}*/CTG* were collected and aged to embryonic stage S13 to S16. In each blot, 50-100st GFP+ or GFP- embryos were used. The selected embryos were homogenized directly in 1xSDS loading buffer (62.5 mM Tris-HCl pH 6.8, 2.5 % SDS, 0.002 % Bromophenol Blue, 0.7135 M (5%) β-mercaptoethanol, 10 % glycerol) and denatured at 98 °C heat blot for 5 min. After centrifuged, supernatant was taken for Western-Blotting with 8% of SDS-PAGE. Rabbit anti-Ham (1:2000) primary antibody was used in blotting. To minimize unspecific signal from IgG heavy chains, light chain specific secondary antibody of mouse anti-Rabbit IgG (1:40000 Jackson ImmunoResearch) was used, and the signals were developed with ECL Plus reagent (GE Healthcare).

Cell culture and Luciferase assays

To generate different variants of Ham, the open reading frames of HamFL, Ham-NZF-vp16, Ham-CZF-vp16, and $ham^{PR\Delta}$ were PCR amplified and cloned into the pAC_V5 (nitrogen) vector. The enhancer fragments were cloned in to the p2xTetO-Firefly luciferase vector. All transfections were performed using *Drosophila* S2-R+ cells grown in Schneider *Drosophila* medium containing 10% fetal calf serum. Cells were co-transfected with the Ham expression construct, 2xTetO-Firefly luciferase and pAc-Renilla plasmids in 96-well plate using the Effectene Transfection kit (Qiagene). Luciferase assays were performed and measured using the Dual Luciferase Assay System (Promega). Expression was calculated as the ratio between

the firefly and *Renilla* luciferase activities. Three rounds of transfections were performed on different days and different cell populations and considered as three biological replicates. Within each biological replicate, 4 wells of cells were transfected with the same DNA mixture and measured and thus considered as 4 technique replicates. In total, for each DNA combination, the values from the 12 wells of transfection were calculated, averaged and plotted in **Fig. 4F-G** and **Supplementary Fig. 6D**. Cloning oligos are provided in **Supplementary table 4**.

SCRINSHOT

The Drosophila reproductive system was dissected at defined ages in 1xPBS and fixed in 4% paraformaldehyde in PBS for 20min. After washing with PBST 0.1% (Triton X-100) for 2 x 15 min, fine dissected samples were placed on Poly-lysine coverslip and freezed at -80°C after drying on a heater.

The SCRINSHOT experiments were carried out according to the published method [55]. In brief, 3 padlock probes and 3 corresponding detection probes were designed for each gene of interest. The slides with fine dissected samples were pretreated at 45°C to reduce moisture and fixed in 4% PFA in 1X PBS, followed by washing in PBS Tween-20 0.05% twice. Samples were then dehydrated with 70%, 85%, 100%ETOH and air dry. The SecureSeal hybridization chamber (GRACE BIO-LABS, 621501) was then mounted to cover samples on the slide. Permeabilization of tissues were first done by treating with 10µg/mL Proteinase K (Invitrogen) in PBSTween-20 0.05% for 7 minutes followed by washing with Glycine (2mg/mL in PBS Tween-20 0.05%) once and with PBS Tween-20 0.05% for 3 x 5 minutes. After this, samples were further Permeabilized in 0.1M HCl for 3min, followed by washing in PBS Tween-20 0.05% twice. Samples were then blocked in a probe-free hybridization reaction mixture of 1XAmplifase buffer (Lucigen, A1905B), 0.05M KCl, 20% Formamide deionized (Millipore S4117), 0.1uM Oligo-dT, 0.1ug/ul BSA (New England Biolabs, B9000S), 1U/ul RiboLock (Thermo, EO0384), and 0.2ug/ul tRNAs (Ambion, AM7119). Then hybridization of padlock probes was done by incubating samples with padlock probes (with the concentration of each one 0.01uM) mixed in blocking reagents used before (no oligo dT used in this step). The slide was then put into a PCR machine to denature at 55˚C for 15 minutes and hybridize at 45˚C for 120 minutes. Padlock probes were then ligated by using SplintR ligase (NEB M0375) at 25˚C for 16 hours followed by RCA (rolling cycle amplification) at 30˚C for 16 hours by using phi29 polymerase (Lucigen, 30221–2) and RCA primer1. Then a fixation step was applied to stabilize RCA product in 4% PFA for 15 minutes followed by washing in PBS Tween-20 0.05%. Then

the hybridization of the first 3 genes was done by mixing all 3 3' fluorophore-conjugated detection probes of each gene in reaction reagent (2XSSC, 20% Formamide deionized, 0.1ug/ul BSA, and 0.5 ng/µl DAPI (Biolegend, 422801) followed by hybridization at 30˚C for 1 hour. The slides were washed in 20% formamide in 2X SSC and then in 6X SSC, followed by dehydration in 70%, 85%, 100% Ethanol until the chamber was removed. Then the samples were preserved in SlowFade Gold Antifade mountnant (Thermo, S36936) and kept in dark before imaging. After image acquisition, the first 3 detection probes were removed by using Uracil-DNA Glycosylase (Thermo, EN0362), and the slides were ready for the next round of detection probe hybridization. The procedure was repeated until all genes were hybridized and imaged. Images were acquired with an airyscan-equipped confocal microscope system (Zeiss LSM 800, Carl Zeiss), and ZEN 2.5 Blue edition software was used for image processing.

Quantification of SCRINSHOT signals

Similar to quantification of immunofluorescent signal, fluorescence intensity of SCRINSHOT for each gene was measured in defined areas within images of the SV, EjD, and TE in 2D projections. Squares were drawn to define areas at the leading side of the SV, the middle region of the Ejd and the TE terminal. The total fluorescence intensity was first normalized to area size. The resultant value for *ham* mutant or RNAi samples was then contrasted to the normalized intensity of control samples.

CUT&TAG

CUT&TAG was performed according to the published method [38]. In brief, TE and grossly tissue of the posterior abdomen were dissected from 18-25h APF *w1118* and *pBAC_ham_sfGFP* animals in PBS within 30 min. For grossly tissues, the dissected samples were homogenized in 2ml NE1 buffer followed by incubation on ice for 10 min. After filtering out the grossly cuticles, nuclei were collected by spinning at 1300xg and resuspended in 1ml PBS. For TE, nuclei extraction was done by simply pipetted samples in 200ul NE1 up and down for 20-30 times and incubated on ice for 10 min. Light fixation was performed with 0.1% formaldehyde at RT for 2 minutes and neutralized with 75mM Glycine. Then the nuclei were washed by PBS and wash buffer 1 time each and kept in 200ul wash buffer on ice until enough samples were collected (30-50st animals per/antibody). Resuspended nuclei in 1.2ml wash buffer and mixed with 20ul Concanavalin A-coated magnetic beads (Polyscience 86057) with soft vortexing. Aliquoted samples into two parts immediately and incubated for 10 min with rotation to allow the binding of the nuclei with the beads. The nuclei/beads mix was then

blocked with 1mL cold antibody buffer for 10 min and resuspended in 150ul cold antibody buffer. For w1118 samples, 1uL Rabbit anti-Ham or 1ul Rabbit IgG (SIGMA-ALDRICH, I5006) was added for an overnight incubation at 4°C. For *pBAC_ham_sfGFP* samples, 1ul Rabbit anti-GFP (G10362, invitrogen) or Rabbit IgG was used. The beads/nuclei/antibody mix was then washed with Dig-wash buffer and incubated with secondary antibody (1:100 dilution) for 1 hour. After further washes with the Dig-wash buffer, a pA-Tn5 adaptor complex in Dig-300 buffer was added to the beads for 1 hour reaction. The beads were then washed with Dig-300 buffer before the incubation with 300ul Tagmentation buffer at 37°C for 1 hour. Then 10ul 0.5M EDTA, 3uL 10% SDS and 2.5uL 20 mg/mL proteinase K (Invitrogen) were used to stop the reaction. Then the resultant DNA was purified with DNA clean & Concentrator kit (ZYMO Research D4013) and eluted in 25uL Elution buffer. To generate libraries, 21uL fragment DNA was mixed with 2uL 10uM Universal i5 primer, 2uL 10uM uniquely barcoded i7 primer and 25uL PCR master mix (NEB Phusion® High-Fidelity PCR Master Mix with HF Buffer, M0531). The PCR condition was as follows: 72°C 5min, 98°C 30s, repeat 12 times (98°C 10s, 63°C 10s), 72°C 1 min and hold 4°C. The libraries were cleaned with standard Ampure XP beads as previously described. Libraries from four biological replicates were produced for each condition.

We mapped the CUT&TAG samples of *w1118* and *pBAC_ham_sfGFP* in TE and TG tissues to the dm6 genome assembly using Bowtie2 with the following parameters: bowtie2 --end-to-end --very-sensitive --no-mixed --no-discordant --phred33 -I 10 -X 700. The coverage for these samples was generated using bedtools genomeCoverageBed and normalized to library depth to yield reads per million per base (RPM). For peak calling, we employed SEACR [67], which is tailored for sparse chromatin profiling data like CUT&TAG. We first used a relaxed FDR cutoff of < 0.5 for each replicate (SEACR_1.3.sh normalized_coverage 0.5 norm stringent output_peaks), we then identified common peaks across replicates for each condition. To select confident peaks for *w1118* and *pBAC_ham_sfGFP*, we overlapped their peaks within TE and TG separately, choosing the top 1800 peaks from TE and the top 6000 from TG. Peak annotation was performed by HOMER's annotatePeaks.pl. Peak overlap analysis was performed using HOMER's mergePeaks function with the default -d given parameter, ensuring that only directly overlapping peaks were merged. This method preserved the integrity of the original peak boundaries and maintained the specified distances between peaks from the initial peak calls. *De novo* motif discovery for peaks in up-regulated or down-regulated genes, positioned 2000 bp upstream and 500 bp downstream of the TSS in TE and TG tissues, was

performed using the MEME-ChIP software. The parameters used were: -ccut 100, -meme-p 5, -dna, -meme-mod anr, -minw 5, -maxw 15, and -filter-thresh 0.05.

RNA-seq

Total RNA was extracted from finely dissected genital discs or testis samples from 18-25h APF animals using Trizol reagent (Invitrogen). RNA quality was tested by Agilent Bioanalyzer.

RNA-seq libraries were made using the Illumina Truseq Total RNA library Prep Kit LT. Sequencing was performed on the Illumina Hiseq2500 platform. Following the trimming of adapter sequences with Trimmomatic, RNA-seq reads from replicated wild type (x3) and mutant samples (x3) were aligned to the *Drosophila melanogaster* (dm6) genome assembly utilizing HISAT2. Gene annotations were sourced from UCSC. The DESeq2 Bioconductor package was employed to identify differentially expressed mRNAs between *w1118* and the $ham^{PR\Delta}/ham^{PR\Delta}$ mutant, as well as between +/Df and ham^{SK1}/Df mutant, with a subsequent estimation of the false discovery rate (FDR). Genes with an FDR < 10% and absolute Log2FC>0 were considered differentially expressed. Details of the calculated differential expression are provided in **Supplementary table 5**.

STRING gene network analyses

Ham activated (genes downregulated in *hamSK1* and bound by Ham in TG) and repressed (genes upregulated in *hamSK1* and bound by Ham in TG) gene networks are constructed using String, MCL clustering (find natural clusters the stochastic flow, inflation parameter, 2. Disconnected genes are hidden. The position of the clusters is manually adjusted to fit related GO categories. The links to the gene networks in STRING:

https://string-db.org/cgi/network?taskId=bbF8IgMTqf1M&sessionId=bzDIAZvMgWsi

https://string-db.org/cgi/network?taskId=bhKCcMoLlbwh&sessionId=bzDIAZvMgWsi

Data availability: All sequencing data produced in this study has been submitted to Gene Expression Omnibus (accession number: GSE290310).

References

1. Bernascone, I., M. Hachimi, and F. Martin-Belmonte, *Signaling Networks in Epithelial Tube Formation.* Cold Spring Harb Perspect Biol, 2017. **9**(12).
2. Chung, S. and D.J. Andrew, *The formation of epithelial tubes.* J Cell Sci, 2008. **121**(Pt 21): p. 3501-4.
3. Samakovlis, C., et al., *Development of the Drosophila tracheal system occurs by a series of morphologically distinct but genetically coupled branching events.* Development, 1996. **122**(5): p. 1395-407.
4. Samakovlis, C., et al., *Genetic control of epithelial tube fusion during Drosophila tracheal development.* Development, 1996. **122**(11): p. 3531-6.
5. Sutherland, D., C. Samakovlis, and M.A. Krasnow, *branchless encodes a Drosophila FGF homolog that controls tracheal cell migration and the pattern of branching.* Cell, 1996. **87**(6): p. 1091-101.
6. Tanaka-Matakatsu, M., et al., *Cadherin-mediated cell adhesion and cell motility in Drosophila trachea regulated by the transcription factor Escargot.* Development, 1996. **122**(12): p. 3697-705.
7. Gervais, L., G. Lebreton, and J. Casanova, *The making of a fusion branch in the Drosophila trachea.* Dev Biol, 2012. **362**(2): p. 187-93.
8. Jacinto, A., A. Martinez-Arias, and P. Martin, *Mechanisms of epithelial fusion and repair.* Nat Cell Biol, 2001. **3**(5): p. E117-23.
9. Vasioukhin, V., et al., *Directed actin polymerization is the driving force for epithelial cell-cell adhesion.* Cell, 2000. **100**(2): p. 209-19.
10. Pai, Y.J., et al., *Epithelial fusion during neural tube morphogenesis.* Birth Defects Res A Clin Mol Teratol, 2012. **94**(10): p. 817-23.
11. Caviglia, S. and S. Luschnig, *Tube fusion: making connections in branched tubular networks.* Semin Cell Dev Biol, 2014. **31**: p. 82-90.
12. de Mello Santos, T. and B.T. Hinton, *We, the developing rete testis, efferent ducts, and Wolffian duct, all hereby agree that we need to connect.* Andrology, 2019. **7**(5): p. 581-587.
13. Jemc, J.C., *Somatic gonadal cells: the supporting cast for the germline.* Genesis, 2011. **49**(10): p. 753-75.
14. Fog, C.K., G.G. Galli, and A.H. Lund, *PRDM proteins: important players in differentiation and disease.* Bioessays, 2012. **34**(1): p. 50-60.
15. Chi, J. and P. Cohen, *The Multifaceted Roles of PRDM16: Adipose Biology and Beyond.* Trends Endocrinol Metab, 2016. **27**(1): p. 11-23.
16. Bard-Chapeau, E.A., et al., *Ecotopic viral integration site 1 (EVI1) regulates multiple cellular processes important for cancer and is a synergistic partner for FOS protein in invasive tumors.* Proc Natl Acad Sci U S A, 2012. **109**(6): p. 2168-73.
17. Zhou, B., et al., *PRDM16 Suppresses MLL1r Leukemia via Intrinsic Histone Methyltransferase Activity.* Mol Cell, 2016.
18. Corrigan, D.J., et al., *PRDM16 isoforms differentially regulate normal and leukemic hematopoiesis and inflammatory gene signature.* J Clin Invest, 2018. **128**(8): p. 3250-3264.

948 19. Cibi, D.M., et al., *Prdm16 Deficiency Leads to Age-Dependent Cardiac Hypertrophy,*
949 *Adverse Remodeling, Mitochondrial Dysfunction, and Heart Failure.* Cell Rep, 2020.
950 **33**(3): p. 108288.
951 20. Kundu, A., et al., *PRDM16 suppresses HIF-targeted gene expression in kidney cancer.*
952 J Exp Med, 2020. **217**(6).
953 21. Horvath, C. and C. Scheele, *PRDM16 stability and metabolically healthy adipose*
954 *tissue.* Nat Metab, 2022. **4**(9): p. 1095-1096.
955 22. Wang, Q., et al., *Post-translational control of beige fat biogenesis by PRDM16*
956 *stabilization.* Nature, 2022. **609**(7925): p. 151-158.
957 23. Hurwitz, E., et al., *Antagonism between Prdm16 and Smad4 specifies the trajectory*
958 *and progression of pancreatic cancer.* J Cell Biol, 2023. **222**(4).
959 24. Moore, A.W., L.Y. Jan, and Y.N. Jan, *hamlet, a binary genetic switch between single-*
960 *and multiple- dendrite neuron morphology.* Science, 2002. **297**(5585): p. 1355-8.
961 25. Moore, A.W., et al., *Conversion of neurons and glia to external-cell fates in the*
962 *external sensory organs of Drosophila hamlet mutants by a cousin-cousin cell-type*
963 *respecification.* Genes Dev, 2004. **18**(6): p. 623-8.
964 26. Rives-Quinto, N., et al., *Sequential activation of transcriptional repressors promotes*
965 *progenitor commitment by silencing stem cell identity genes.* Elife, 2020. **9**.
966 27. Eroglu, E., et al., *SWI/SNF complex prevents lineage reversion and induces temporal*
967 *patterning in neural stem cells.* Cell, 2014. **156**(6): p. 1259-73.
968 28. Endo, K., et al., *Chromatin modification of Notch targets in olfactory receptor neuron*
969 *diversification.* Nat Neurosci, 2012. **15**(2): p. 224-33.
970 29. Pinheiro, I., et al., *Prdm3 and Prdm16 are H3K9me1 methyltransferases required for*
971 *mammalian heterochromatin integrity.* Cell, 2012. **150**(5): p. 948-60.
972 30. Hohenauer, T. and A.W. Moore, *The Prdm family: expanding roles in stem cells and*
973 *development.* Development, 2012. **139**(13): p. 2267-82.
974 31. Gokcezade, J., G. Sienski, and P. Duchek, *Efficient CRISPR/Cas9 plasmids for rapid and*
975 *versatile genome editing in Drosophila.* G3 (Bethesda), 2014. **4**(11): p. 2279-82.
976 32. DeFalco, T., S. Le Bras, and M. Van Doren, *Abdominal-B is essential for proper*
977 *sexually dimorphic development of the Drosophila gonad.* Mech Dev, 2004. **121**(11):
978 p. 1323-33.
979 33. Whitworth, C., E. Jimenez, and M. Van Doren, *Development of sexual dimorphism in*
980 *the Drosophila testis.* Spermatogenesis, 2012. **2**(3): p. 129-136.
981 34. Ahmad, S.M. and B.S. Baker, *Sex-specific deployment of FGF signaling in Drosophila*
982 *recruits mesodermal cells into the male genital imaginal disc.* Cell, 2002. **109**(5): p.
983 651-61.
984 35. Rothenbusch-Fender, S., et al., *Myotube migration to cover and shape the testis of*
985 *Drosophila depends on Heartless, Cadherin/Catenin, and myosin II.* Biol Open, 2017.
986 **6**(12): p. 1876-1888.
987 36. Bischoff, M.C., et al., *Filopodia-based contact stimulation of cell migration drives*
988 *tissue morphogenesis.* Nature Communications, 2021. **12**(1): p. 791.
989 37. Jenett, A., et al., *A GAL4-driver line resource for Drosophila neurobiology.* Cell Rep,
990 2012. **2**(4): p. 991-1001.
991 38. Kaya-Okur, H.S., et al., *CUT&Tag for efficient epigenomic profiling of small samples*
992 *and single cells.* Nat Commun, 2019. **10**(1): p. 1930.

39. Szklarczyk, D., et al., *The STRING database in 2023: protein-protein association networks and functional enrichment analyses for any sequenced genome of interest.* Nucleic Acids Res, 2023. **51**(D1): p. D638-D646.
40. Kozopas, K.M., C.H. Samos, and R. Nusse, *DWnt-2, a Drosophila Wnt gene required for the development of the male reproductive tract, specifies a sexually dimorphic cell fate.* Genes Dev, 1998. **12**(8): p. 1155-65.
41. Deshpande, G., A. Nouri, and P. Schedl, *Wnt Signaling in Sexual Dimorphism.* Genetics, 2016. **202**(2): p. 661-73.
42. van Impel, A., et al., *Regulation of the Rac GTPase pathway by the multifunctional Rho GEF Pebble is essential for mesoderm migration in the Drosophila gastrula.* Development, 2009. **136**(5): p. 813-22.
43. Oda, H., et al., *A Drosophila homolog of cadherin associated with armadillo and essential for embryonic cell-cell adhesion.* Dev Biol, 1994. **165**(2): p. 716-26.
44. Ferrante, A.W., Jr., R. Reinke, and E.R. Stanley, *Shark, a Src homology 2, ankyrin repeat, tyrosine kinase, is expressed on the apical surfaces of ectodermal epithelia.* Proc Natl Acad Sci U S A, 1995. **92**(6): p. 1911-5.
45. Gonzalez-Gaitan, M. and H. Jackle, *Role of Drosophila alpha-adaptin in presynaptic vesicle recycling.* Cell, 1997. **88**(6): p. 767-76.
46. Weber, A.N., et al., *Binding of the Drosophila cytokine Spatzle to Toll is direct and establishes signaling.* Nat Immunol, 2003. **4**(8): p. 794-800.
47. Staubli, F., et al., *Molecular identification of the insect adipokinetic hormone receptors.* Proc Natl Acad Sci U S A, 2002. **99**(6): p. 3446-51.
48. Kawamura, K., et al., *A new family of growth factors produced by the fat body and active on Drosophila imaginal disc cells.* Development, 1999. **126**(2): p. 211-9.
49. Lam, G.T., C. Jiang, and C.S. Thummel, *Coordination of larval and prepupal gene expression by the DHR3 orphan receptor during Drosophila metamorphosis.* Development, 1997. **124**(9): p. 1757-69.
50. Prokopenko, S.N., et al., *A putative exchange factor for Rho1 GTPase is required for initiation of cytokinesis in Drosophila.* Genes Dev, 1999. **13**(17): p. 2301-14.
51. Nakamura, M., J.M. Verboon, and S.M. Parkhurst, *Prepatterning by RhoGEFs governs Rho GTPase spatiotemporal dynamics during wound repair.* J Cell Biol, 2017. **216**(12): p. 3959-3969.
52. Lin, Y.H., et al., *AP-2-complex-mediated endocytosis of Drosophila Crumbs regulates polarity by antagonizing Stardust.* J Cell Sci, 2015. **128**(24): p. 4538-49.
53. Campbell, K. and J. Casanova, *A role for E-cadherin in ensuring cohesive migration of a heterogeneous population of non-epithelial cells.* Nat Commun, 2015. **6**: p. 7998.
54. Chen, H., et al., *E-cadherin mediates adhesion and suppresses cell motility via distinct mechanisms.* J Cell Sci, 1997. **110 (Pt 3)**: p. 345-56.
55. Sountoulidis, A., et al., *SCRINSHOT enables spatial mapping of cell states in tissue sections with single-cell resolution.* PLoS Biol, 2020. **18**(11): p. e3000675.
56. Lee, M., et al., *Distinct sites in E-cadherin regulate different steps in Drosophila tracheal tube fusion.* Development, 2003. **130**(24): p. 5989-99.
57. Lee, S. and P.A. Kolodziej, *The plakin Short Stop and the RhoA GTPase are required for E-cadherin-dependent apical surface remodeling during tracheal tube fusion.* Development, 2002. **129**(6): p. 1509-20.
58. Umetsu, D., *Cell mechanics and cell-cell recognition controls by Toll-like receptors in tissue morphogenesis and homeostasis.* Fly (Austin), 2022. **16**(1): p. 233-247.

59. Karlsson, M., et al., *A single-cell type transcriptomics map of human tissues.* Sci Adv, 2021. **7**(31).
60. Corty, M.M., B.J. Matthews, and W.B. Grueber, *Molecules and mechanisms of dendrite development in Drosophila.* Development, 2009. **136**(7): p. 1049-61.
61. Araujo, S.J. and J. Casanova, *Sequoia establishes tip-cell number in Drosophila trachea by regulating FGF levels.* J Cell Sci, 2011. **124**(Pt 14): p. 2335-40.
62. Brenman, J.E., et al., *Sequoia, a tramtrack-related zinc finger protein, functions as a pan-neural regulator for dendrite and axon morphogenesis in Drosophila.* Dev Cell, 2001. **1**(5): p. 667-77.
63. Araujo, S.J., C. Cela, and M. Llimargas, *Tramtrack regulates different morphogenetic events during Drosophila tracheal development.* Development, 2007. **134**(20): p. 3665-76.
64. Li, S., et al., *Photoreceptor cell differentiation requires regulated proteolysis of the transcriptional repressor Tramtrack.* Cell, 1997. **90**(3): p. 469-78.
65. Pitsouli, C. and N. Perrimon, *The homeobox transcription factor cut coordinates patterning and growth during Drosophila airway remodeling.* Sci Signal, 2013. **6**(263): p. ra12.
66. Grueber, W.B., L.Y. Jan, and Y.N. Jan, *Different levels of the homeodomain protein cut regulate distinct dendrite branching patterns of Drosophila multidendritic neurons.* Cell, 2003. **112**(6): p. 805-18.
67. Meers, M.P., D. Tenenbaum, and S. Henikoff, *Peak calling by Sparse Enrichment Analysis for CUT&RUN chromatin profiling.* Epigenetics Chromatin, 2019. **12**(1): p. 42.

Declaration of the use of AI. ChatGPT was used to improve readability of the text, and the content was thoroughly checked and edited by the authors to ensure accuracy.

Figure legends

Figure 1. *ham* is expressed and required for *Drosophila* male RS development

(**A**). The adult male RS. TE, testis; SV, seminal vesicle; AG, accessory gland; EJD, ejaculatory duct. (**B**). White-field images of adult male RS, showing defective morphology in the *ham* mutants. (**C**). Quantification of male fertility. Ham_sfGFP with the *ham* genomic region was used to rescue the sterility. Statistical significance was calculated using unpaired t-test (***, $p<0.001$; **, $p< 0.01$; *, $p<0.05$; n.s., non-significant). (**D**). Images of the adult RS stained with Ham_V5 in red. DNA is stained with DAPI in blue. The blue and white dashed lines highlight the TE and SV respectively. (**E**). Illustration of the developing male RS at the larval stage. The testis (TE) terminal epithelial cells localize at the opposite side of the germline stem cell (GSC) niche. The genital disc (GD) contains mesenchymal cells (MC) that will develop into the SV and accessory gland (ag). (**F**). Images of the larval TE (top) and GD (bottom) stained with Ham_V5 in red or magenta, the reporter in lime-green (btlGal4 driving UAS-GFP) and DAPI in blue. AEL, after egg laying. (**G**). Illustration of the TE and SV fusion process. APF, after pupal formation. (**H**). Images of the pupal GD stained with Ham_V5 in magenta, the reporter in lime-green (btlGal4 driving UAS-GFP) and DAPI in blue. (**I**) Images of the pupal RS with Ham_V5 in red and DAPI in blue. The blue and white dashed lines highlight the TE and SV respectively. (**J**). Higher magnification image of the joint site between the SV and TE, with myoblasts and myotubes labeled by mef2Gal4>GFP in lime-green.

Figure 2. Ham promotes differentiation of the TE terminal and SV epithelial cells

(**A**). Images of the male RS at the pupal stage, showing morphological defects of the TE and SV in the ham mutants. Epithelial cells are labeled with Coracle (Cor). The phenotype penetrance (%) and number of animals (n) counted are indicated as % (n). (**B**). High magnification images of the connection site of the TE and SV, showing that the ham mutant RS failed to form a continuous tube. Ham-sfGFP restored the normal morphology. Epithelial cells are marked by E-Cad in red, Cor in yellow, and the epithelium on the SV side also marked by btlGal4 driving UAS-mCD8GFP. DNA is labeled by DAPI in blue. (**C**). Images and quantification of the E-Cad signal in the *wt* and *hamPRΔ* mutant SV. (**D**). Images and quantification of the Crumbs signal in the *wt* and *hamPRΔ /Df* mutant SV. (**E**). Images and quantification of the length of Cor signal in the wt and *hamPRΔ* mutant SV. (**F**) Images of *ham* mutant mosaic clones in the TE terminal epithelial cells. Note, the mutant cells are GFP

negative and within the area surrounded by the white dashed line. The white arrows indicate junctions between mutant cells, while the yellow arrows highlight the junctions between wild-type cells. (**G**). Images of pupal male GD, showing that *hamRNAi*-mediated knockdown reproduces *ham* mutant phenotypes. (**H**). Images of pupal male RS, stained with E-Cad in red, Ham in yellow, GFP in green and DAPI in blue. UAS-dcr2 enhanced knockdown efficiency and led to more severe morphological defects. (**I**). Images and quantification of E-Cad signal in red and Cor length in blue in control and ham RNAi SV. (**J**) Images and quantification of E-Cad signal in control and ham RNAi TE terminal epithelium. Statistical significance was calculated using unpaired t-test except for TE mosaic clones which used paired t-test. (***, $p<0.001$; **, $p< 0.01$; *, $p<0.05$; ns, non-significant).

Figure 3. Identification of Ham-regulated genes in the developing TE and GD

(**A**). Illustration of the sample types and antibodies used in the RNA-seq and CUT&TAG experiments. (**B**) Venn diagram of dysregulated genes between the two mutant conditions in the GD (left) and TE (right) samples. (**C**) Heatmaps of Ham CUT&TAG peak density and IgG control, ranked from high to low and centered at peak summits. (**D**) Venn diagrams of CUT&TAG peaks from the two types of samples. (**E-F**). Volcano plots of dysregulated genes in GD (E) and TE (F) in the *hamSK1/Df* mutant, and the ones with at least one Ham CUT&TAG peak are highlighted.

Figure 4. Ham activates expression of epithelial differentiation genes

(**A**) Ham gene network analysis from STRING. The position of MCL Clusters were manually adjusted to place genes with similar function in close proximity. The functional categories were determined by gene function tools in STRING. (**B**). A bar plot of the Log2 fold-change value from RNA-seq for *wnt2*, *shot* and *shg*, showing downregulation of these genes in the *hamSK1/Df* mutant. (**C**). Schemes of the Ham_FL and other truncation proteins, and illustration of the luciferase reporter assay. (**D-E**). A genome browser snapshot of the *shg* and *wnt2* loci, showing the CUT&TAG tracks from the TE and GD (TG) mixed samples and the enhancer fragments in the luciferase assays. (**F-G**). Normalized luciferase activity to the empty reporter and then to the control vector that expresses GFP and RFP proteins. Statistical significance was calculated using unpaired t-test (****, $p<0.0001$; ***, $p<0.001$; **, $p< 0.01$; *, $p<0.05$; ns, non-significant).

Figure 5. A candidate RNAi screen identified Ham-downstream effectors in RS epithelial tissue fusion

(**A**). Scheme for the RNAi screen. (**B**) Summary of positive hits. The extent of sterility is determined by the number of progenies from the F1 male crossing to the wild-type female (see Methods). 100% means no progeny. >70%, the number of progenies being fewer than 30% of the number of progenies produced by the control cross (the same Gal4 driver x UAS-GFPRNAi). 40-70%, the number of progenies being between 30-60% of the number of progenies produced by the control. (**C**). Images of the control and gene-specific RNAi knockdown RS. The left panels show the fusion site stained with E-Cad in magenta, GFP in lime-green, Ham in grey and DAPI in blue, the middle panels are GD, and the right ones are TE. The orange arrows indicate mobilized epithelial cells in the *shg* knockdown TE.

Figure 6. Spatial-temporal expression dynamics of Ham-downstream genes

(**A**). Images from multiplexed in situ hybridization (the SCRINSHOT method), showing mRNA signal of the indicated genes in *wt* TE samples. DNA is marked by DAPI in grey. (**B**). Images from SCRINSHOT, showing mRNA signals of indicated genes in *wt/Df* and *hamSK1/Df* mutant GD. The last panel is an enlarged view from the sample with *Tl*, *ham* and *spz* probes. The yellow arrowheads indicate myoblast cells with Tl signal. (**C**). Quantification of signal intensity for genes shown in B in two areas, the SV and EjD. Statistical significance was calculated using unpaired t-test (***, $p<0.001$; **, $p< 0.01$; *, $p<0.05$; ns, non-significant). (**D**) Images from SCRINSHOT, showing mRNA signals of indicated genes in *GFP* and *ham RNAi* GD samples. (**E**). Quantification of signal intensity for genes shown in D in two areas, the SV and EjD. (**F**). A summary of genes expressed in the TE terminal and SV epithelium. Highlighted genes show temporal or spatial dynamic expression in the two tissues. Statistical significance was calculated using unpaired t-test (****, $p<0.0001$; ***, $p<0.001$; **, $p< 0.01$; *, $p<0.05$; ns, non-significant).

Figure 7. Wnt2 and its ligand genes are required for male fertility and RS development

(**A**) Images of *wnt2o* mutant TE and GD, showing disrupted morphology in these tissues. (**B**). Images of the TE and SV fusion site from the control and *wnt2* overexpression animals. The epithelial cells of the TE and SV are labeled with hamRSGal4 driving UAS-mCD8GFP in

lime-green and E-Cad in magenta and Ham in grey. The white arrows indicate mobilized GFP positive cells in the middle of the TE, and these cells have a lower level of E-Cad. The blue and white dashed lines highlight the TE and SV respectively. (**C**). Images of the TE and SV fusion site from the control and *fz2* RNAi animals. The white arrows indicate mobilized GFP positive cells in the middle of the TE, and these cells have a lower level of E-Cad. (**D**) Graphs of progeny number from male fertility tests for *fz* and *fz2* RNAi lines in comparison to GFP RNAi. Number of tested males in each genotype, 3. (**E**) Illustration of cell-cell interactions in the developing RS, and a speculated model for Tl and Wnt2 signaling functions. Wnt2 signaling may be involved in epithelial cell interaction between the two ends. Tl signaling and Tl may be involved in the interaction between epithelial cells and myoblasts/myotubes. In three conditions (*shgRNAi*, *wnt2OE* and *fz2RNAi*), some TE terminal epithelial cells (illustrated in orange) move up to the distal end of the testis.

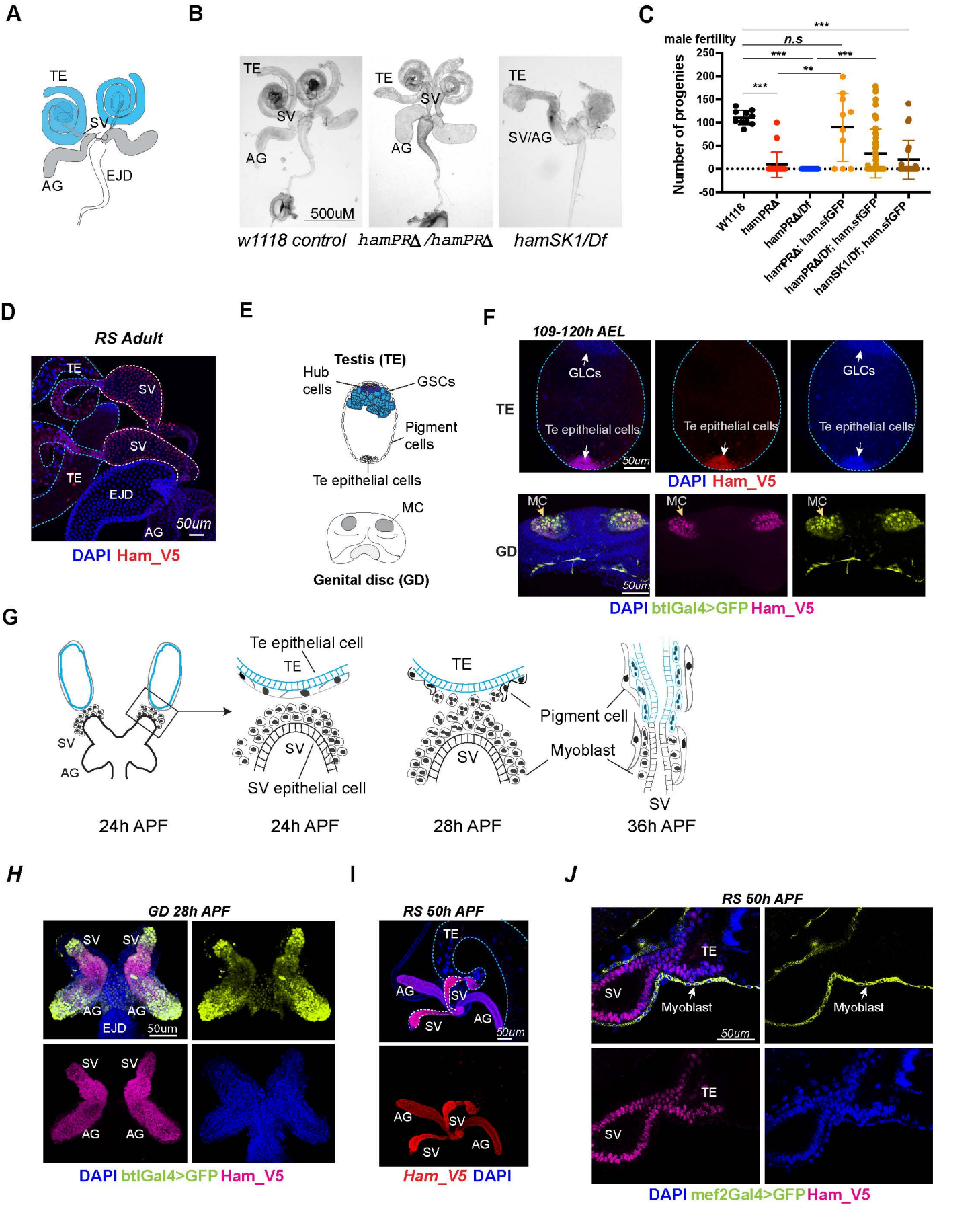
A
TE
SV
EJD
AG
B
TE
SV
AG
500uM
TE
SV
AG
TE
SV/AG
w1118 control
hamPRΔ/hamPRΔ
hamSK1/Df
C
male fertility
n.s
***
**
Number of progenies
250
200
150
100
50
0
-50
W1118
hamPRΔ
hamPRΔ/Df
hamPRΔ; ham.sfGFP
hamPRΔ/Df; ham.sfGFP
hamSK1/Df; ham.sfGFP
D
RS Adult
TE
SV
SV
TE
EJD
AG
50um
DAPI Ham_V5
E
Testis (TE)
Hub cells
GSCs
Pigment cells
Te epithelial cells
MC
Genital disc (GD)
F
109-120h AEL
TE
GLCs
Te epithelial cells
50um
DAPI Ham_V5
GD
MC
50um
DAPI btlGal4>GFP Ham_V5
G
SV
AG
Te epithelial cell
TE
SV
SV epithelial cell
TE
SV
Pigment cell
Myoblast
SV
24h APF
24h APF
28h APF
36h APF
H
GD 28h APF
SV
SV
AG
AG
EJD
50um
SV
SV
AG
AG
DAPI btlGal4>GFP Ham_V5
I
RS 50h APF
TE
AG
SV
SV
AG
50um
AG
SV
SV
AG
Ham_V5 DAPI
J
RS 50h APF
TE
SV
Myoblast
50um
Myoblast
TE
SV
DAPI mef2Gal4>GFP Ham_V5

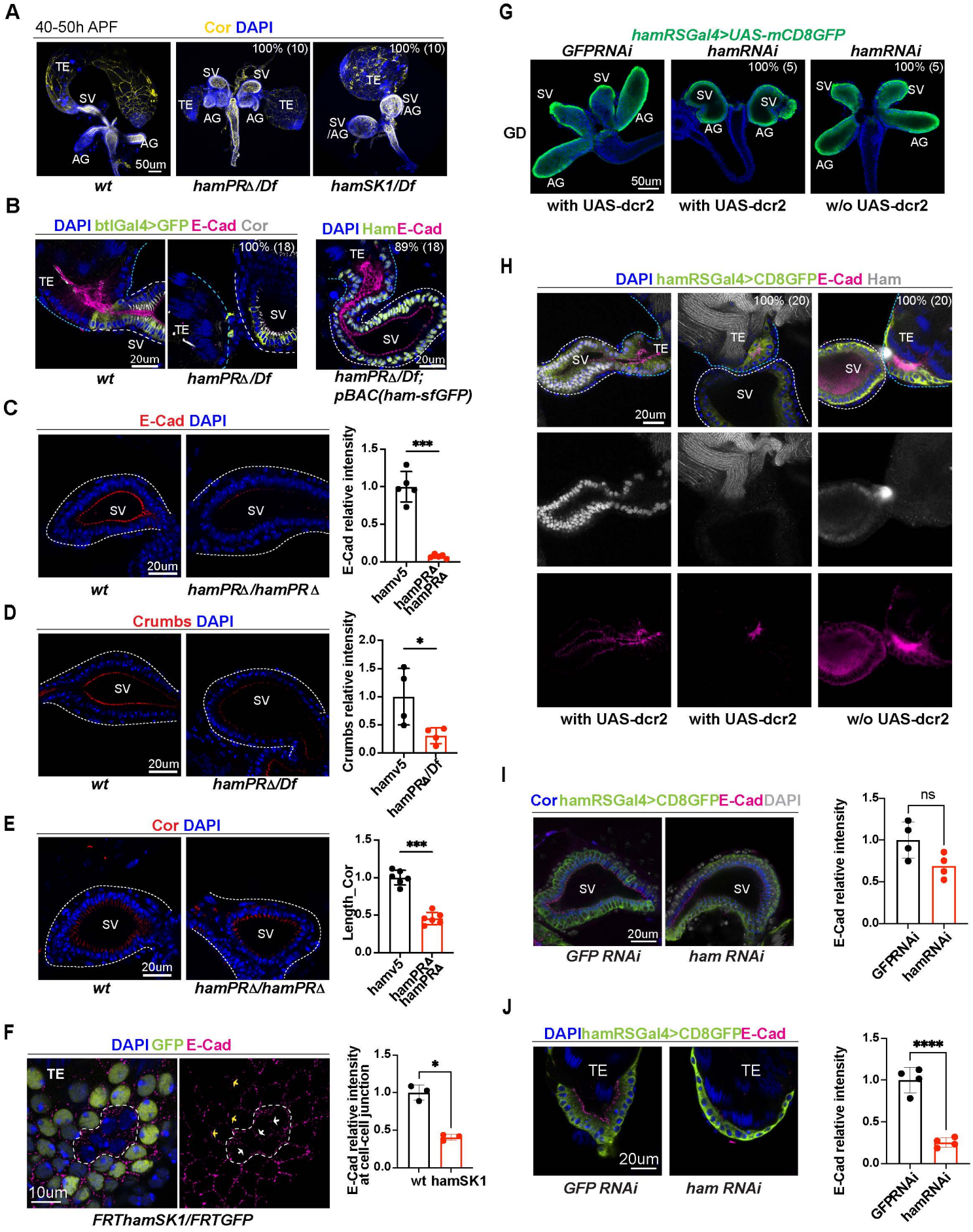
A
40-50h APF
Cor DAPI
TE
SV
AG
50um
100% (10)
wt
hamPRΔ/Df
hamSK1/Df
B
DAPI btlGal4>GFP E-Cad Cor
100% (18)
20um
DAPI Ham E-Cad
89% (18)
hamPRΔ/Df; pBAC(ham-sfGFP)
C
E-Cad DAPI
hamPRΔ/hamPRΔ
E-Cad relative intensity
***
hamv5
hamPRΔ hamPRΔ
D
Crumbs DAPI
Crumbs relative intensity
*
hamPRΔ/Df
E
Cor DAPI
Length_Cor
F
DAPI GFP E-Cad
10um
FRThamSK1/FRTGFP
E-Cad relative intensity at cell-cell junction
wt hamSK1
G
hamRSGal4>UAS-mCD8GFP
GFPRNAi
hamRNAi
GD
100% (5)
with UAS-dcr2
w/o UAS-dcr2
H
DAPI hamRSGal4>CD8GFP E-Cad Ham
100% (20)
I
Cor hamRSGal4>CD8GFP E-Cad DAPI
GFP RNAi
ham RNAi
ns
GFPRNAi
hamRNAi
J
DAPI hamRSGal4>CD8GFP E-Cad
****

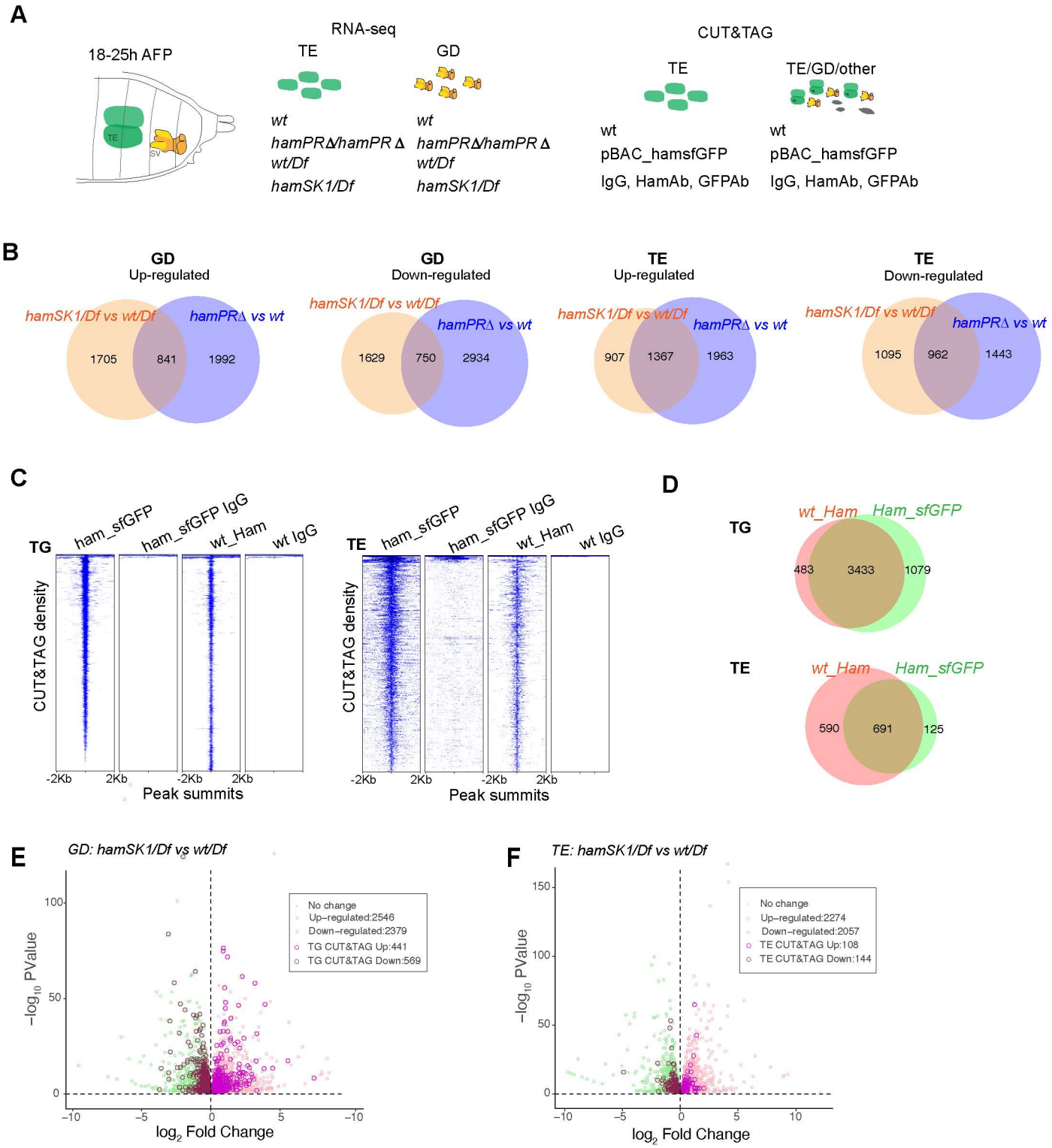
A
18-25h AFP
TE
SV
RNA-seq
TE
GD
wt
hamPRΔ/hamPRΔ
wt/Df
hamSK1/Df
wt
hamPRΔ/hamPRΔ
wt/Df
hamSK1/Df
CUT&TAG
TE
TE/GD/other
wt
pBAC_hamsfGFP
IgG, HamAb, GFPAb
wt
pBAC_hamsfGFP
IgG, HamAb, GFPAb
B
GD
Up-regulated
hamSK1/Df vs wt/Df
hamPRΔ vs wt
1705
841
1992
GD
Down-regulated
hamSK1/Df vs wt/Df
hamPRΔ vs wt
1629
750
2934
TE
Up-regulated
hamSK1/Df vs wt/Df
hamPRΔ vs wt
907
1367
1963
TE
Down-regulated
hamSK1/Df vs wt/Df
hamPRΔ vs wt
1095
962
1443
C
TG
ham_sfGFP
ham_sfGFP IgG
wt_Ham
wt IgG
CUT&TAG density
-2Kb
2Kb
Peak summits
TE
ham_sfGFP
ham_sfGFP IgG
wt_Ham
wt IgG
CUT&TAG density
-2Kb
2Kb
Peak summits
D
TG
wt_Ham
Ham_sfGFP
483
3433
1079
TE
wt_Ham
Ham_sfGFP
590
691
125
E
GD: hamSK1/Df vs wt/Df
No change
Up–regulated:2546
Down–regulated:2379
TG CUT&TAG Up:441
TG CUT&TAG Down:569
−log10 PValue
log2 Fold Change
F
TE: hamSK1/Df vs wt/Df
No change
Up–regulated:2274
Down–regulated:2057
TE CUT&TAG Up:108
TE CUT&TAG Down:144
−log10 PValue
log2 Fold Change

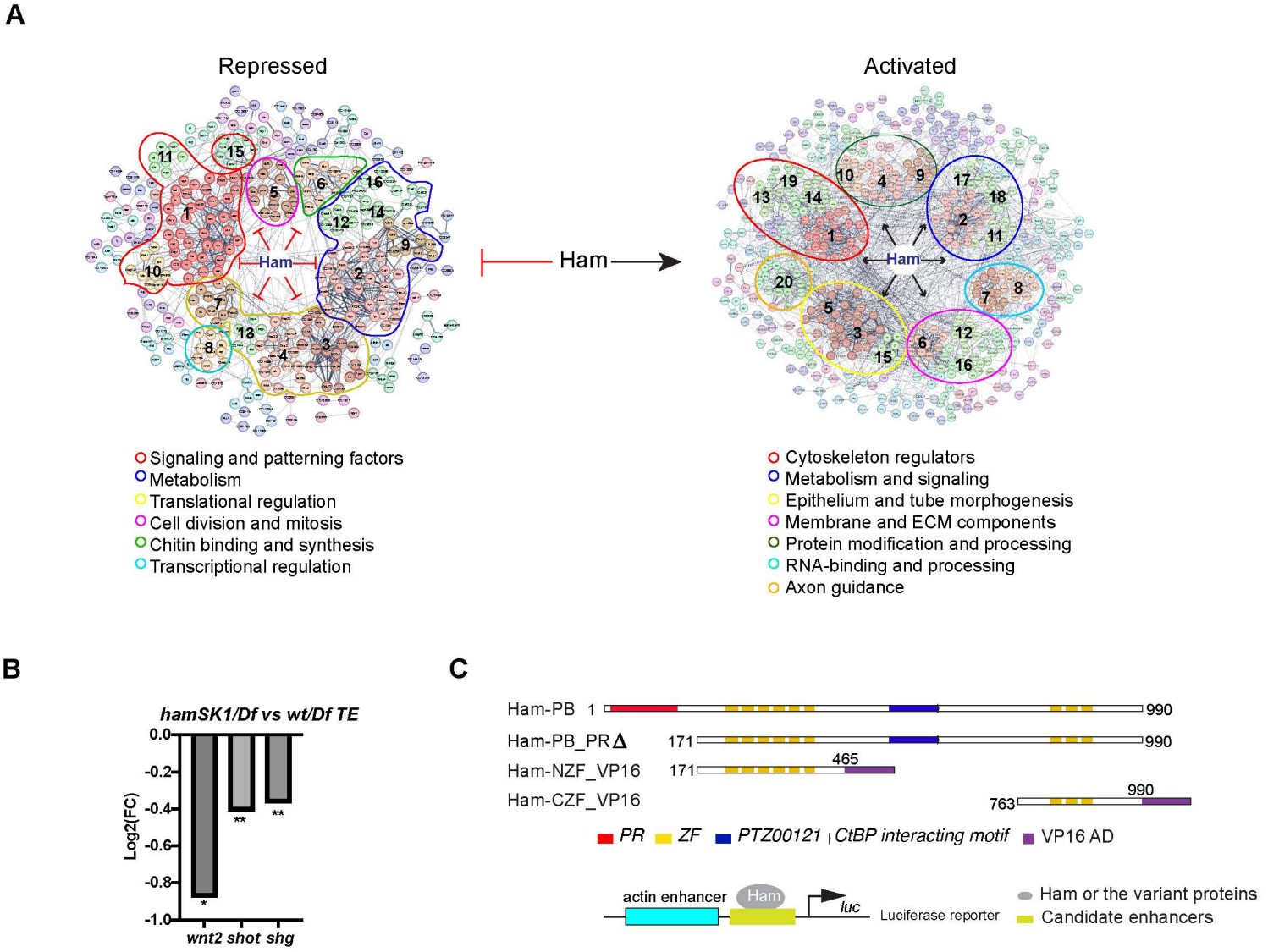
A
Repressed
Activated
Ham
Ham
Signaling and patterning factors
Metabolism
Translational regulation
Cell division and mitosis
Chitin binding and synthesis
Transcriptional regulation
Cytoskeleton regulators
Metabolism and signaling
Epithelium and tube morphogenesis
Membrane and ECM components
Protein modification and processing
RNA-binding and processing
Axon guidance
B
hamSK1/Df vs wt/Df TE
Log2(FC)
wnt2 shot shg
C
Ham-PB 1 990
Ham-PB_PRΔ 171 990
Ham-NZF_VP16 171 465
Ham-CZF_VP16 763 990
PR ZF PTZ00121 CtBP interacting motif VP16 AD
actin enhancer Ham luc Luciferase reporter
Ham or the variant proteins
Candidate enhancers
D
shg_enh2-1
5 kb
shg
CG15653
cpa
HamGFP_TG1_GFP
HamGFP_TG2_GFP
wt_TG2_Ham
E
wnt2_enh1-4
5 kb
wnt2
HamGFP_TG1_GFP
HamGFP_TG2_GFP
wt_TG2_Ham
F
Normalized luciferase activity
GFP-RFP
Ham_FL
Ham_PRdel
Ham_NZF_VP16
Ham_CZF_VP16
shg_enh1
enh2
G
Normalized luciferase activity
GFP-RFP
Ham_FL
Ham_PRdel
Ham_NZF_VP16
Ham_CZF_VP16
wnt2_enh1
enh2
enh3
enh4

A

hamRSGal4>UAS-dcr2; UAS-mCD8GFP

X

UAS-RNAi
(135 lines for 113 genes)

↓

Screen for F1 male sterility

↓

26 positive gene hits

B

Sterility	Genes
100%	*pbl, AP-2alpha, CG11406, shg*
>70%	*GstE11, CG7456, Gr64c, AkhR, Idgf4*
40%-70%	*CG17477, CG11069, CG17186, CG4872, AdsL, Tl, CG17283, decay, PH4alphaMP, Hr46, CG15117, gsb-n, shark, CG17018, cag, CG7484, CG31935*

C

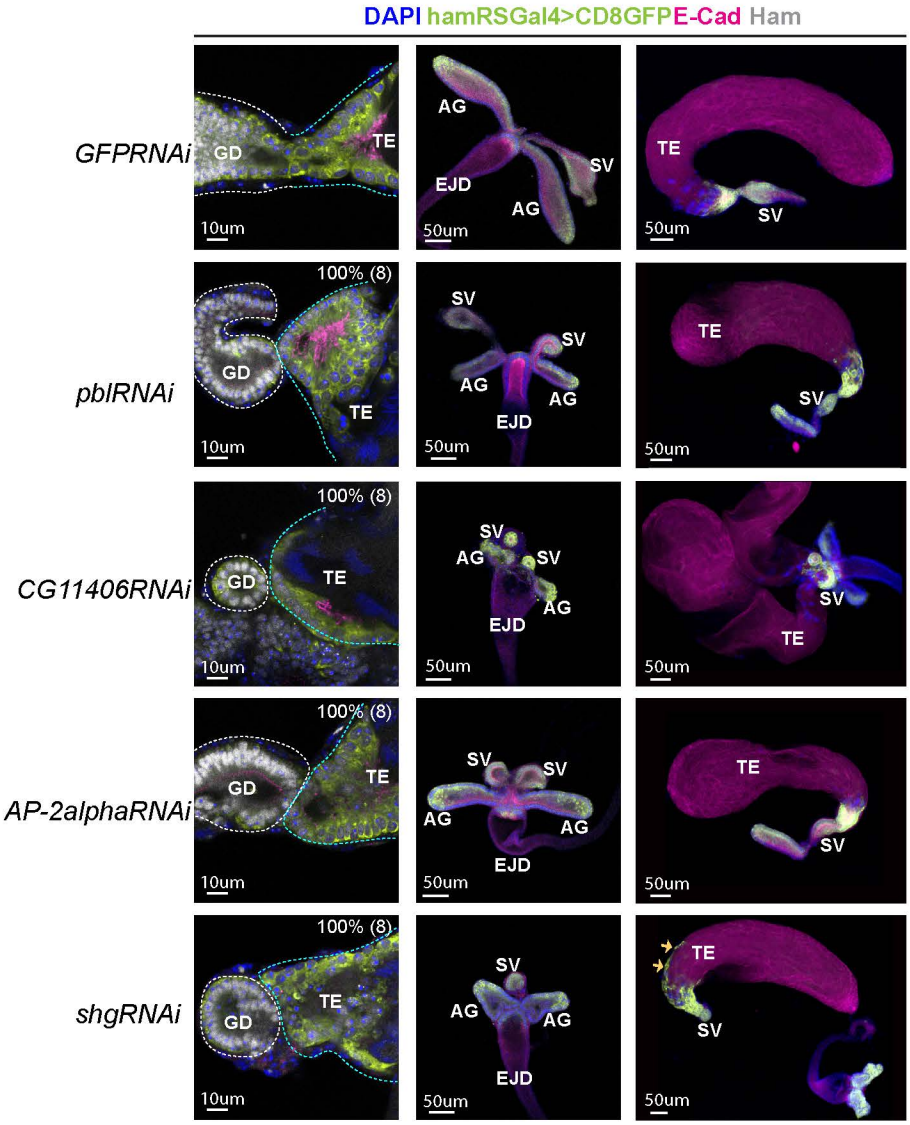

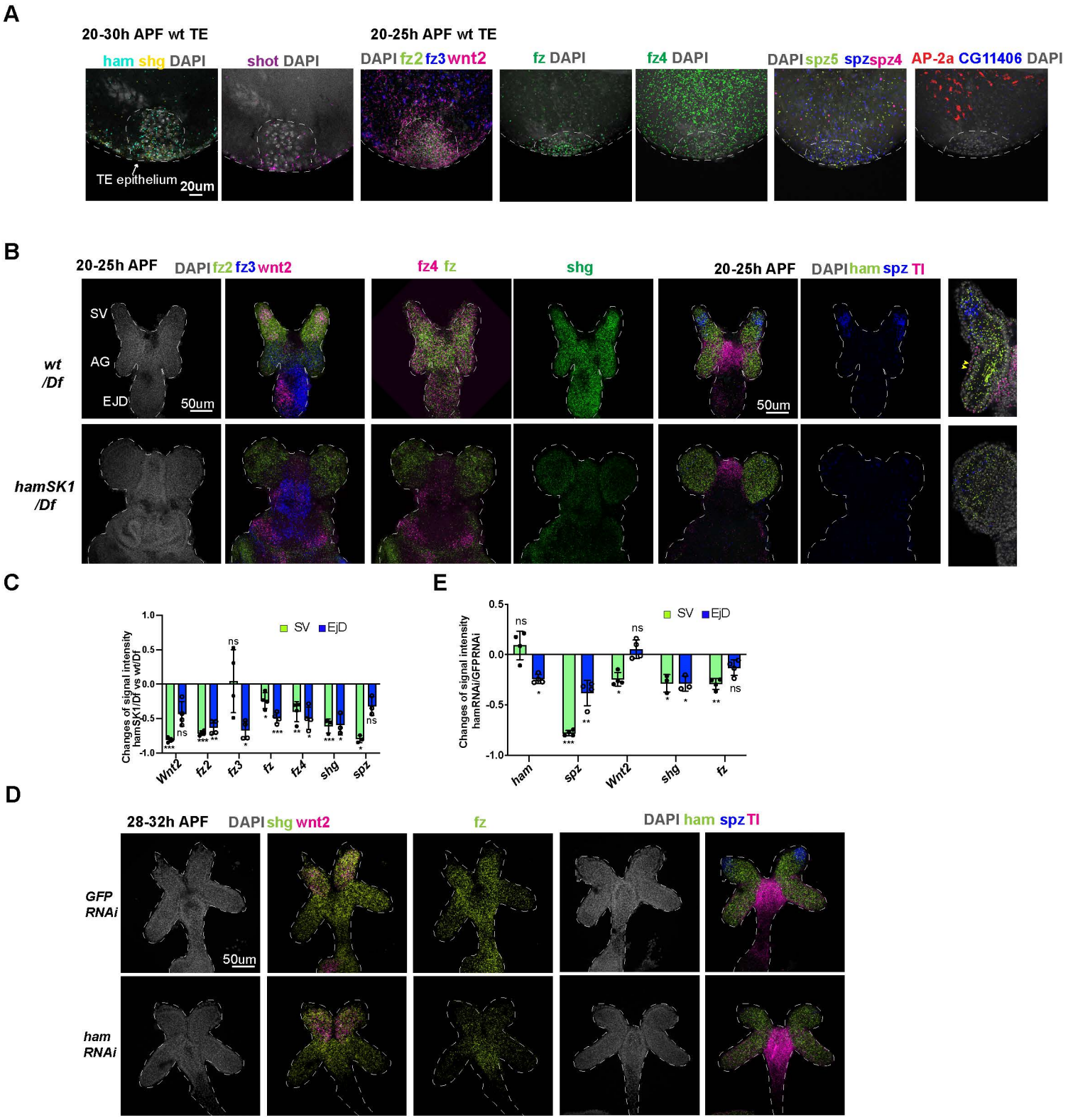
A
20-30h APF wt TE
ham shg DAPI
shot DAPI
20-25h APF wt TE
DAPI fz2 fz3 wnt2
fz DAPI
fz4 DAPI
DAPI spz5 spzspz4
AP-2a CG11406 DAPI
TE epithelium
20um
B
20-25h APF
DAPI fz2 fz3 wnt2
fz4 fz
shg
20-25h APF
DAPI ham spz Tl
SV
AG
EJD
50um
wt /Df
hamSK1 /Df
C
SV EjD
Changes of signal intensity hamSK1/Df vs wt/Df
Wnt2
fz2
fz3
fz
fz4
shg
spz
E
SV EjD
Changes of signal intensity hamRNAi/GFPRNAi
ham
spz
Wnt2
shg
fz
D
28-32h APF
DAPI shg wnt2
fz
DAPI ham spz Tl
GFP RNAi
ham RNAi
50um
F
TE
SV
Tl
TE epithelium
Constant genes:
ham, shg, shot, wnt2, fz, fz2, fz4, spz, AdSL, Shark, CG7456
Early genes:
spz5, CG11406
Late genes:
Tl, spz6, Ap2-a, GstE11
SV epithelium
Shared with TE:
ham, shg, shot, wnt2, fz, fz2, fz4, spz, spz6, AdSL, Shark, spz5, CG7456, GstE11, AP2-a, CG11406
Unique in SV:
CG11069, CG31935,CG17186, fz3, spz4, Gr64c, Cag, CG7484

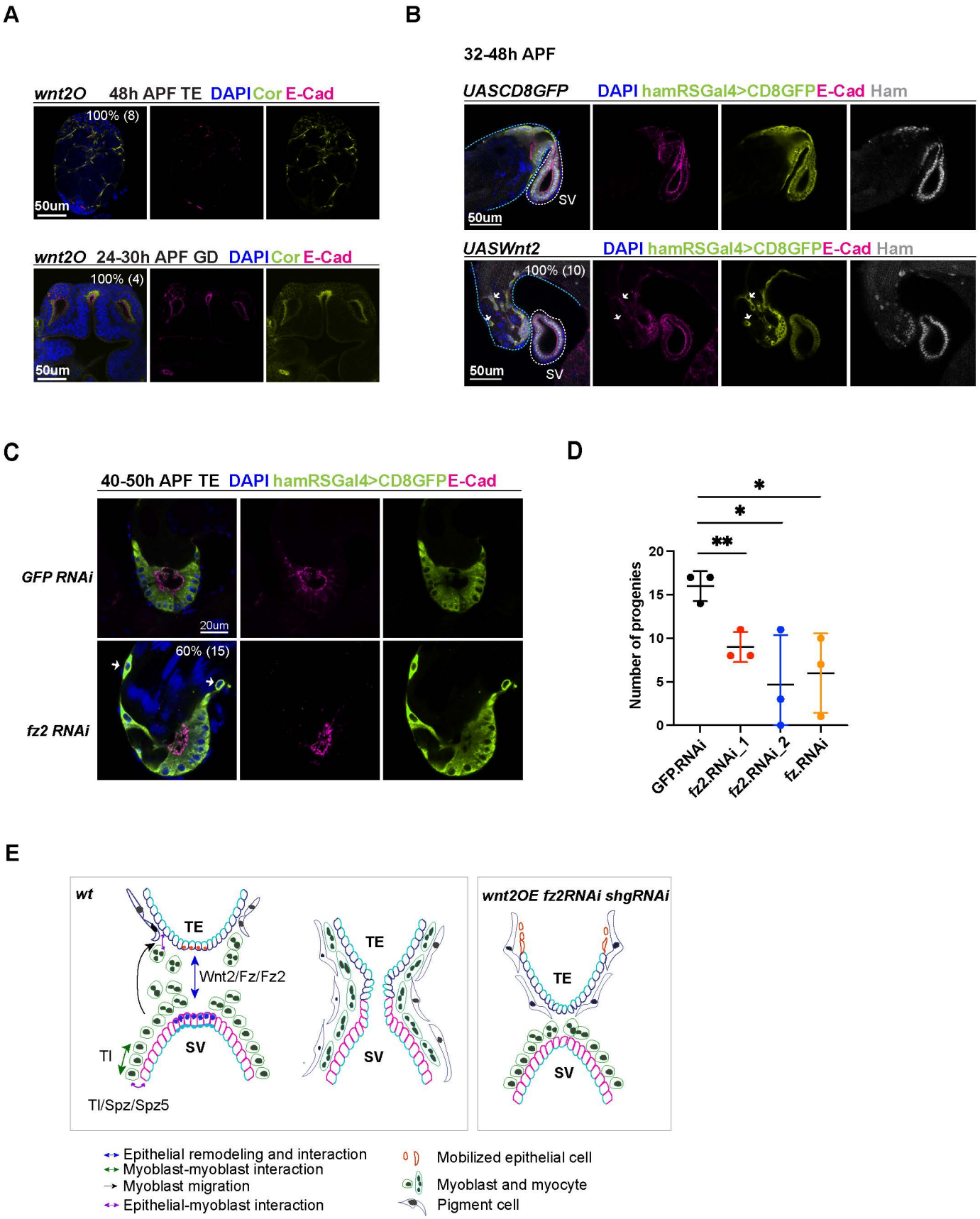
A
wnt2O 48h APF TE DAPI Cor E-Cad
100% (8)
50um
wnt2O 24-30h APF GD DAPI Cor E-Cad
100% (4)
50um
B
32-48h APF
UASCD8GFP DAPI hamRSGal4>CD8GFP E-Cad Ham
SV
50um
UASWnt2 DAPI hamRSGal4>CD8GFP E-Cad Ham
100% (10)
50um
SV
C
40-50h APF TE DAPI hamRSGal4>CD8GFP E-Cad
GFP RNAi
20um
60% (15)
fz2 RNAi
D
Number of progenies
20
15
10
5
0
*
*
**
GFP.RNAi
fz2.RNAi_1
fz2.RNAi_2
fz.RNAi
E
wt
TE
Wnt2/Fz/Fz2
SV
Tl
Tl/Spz/Spz5
TE
SV
wnt2OE fz2RNAi shgRNAi
TE
SV
Epithelial remodeling and interaction
Myoblast-myoblast interaction
Myoblast migration
Epithelial-myoblast interaction
Mobilized epithelial cell
Myoblast and myocyte
Pigment cell

Supplementary figure legend

Suppl._Figure 1. Ham gene locus and mutant alleles.

(**A**) Illustration of the ham genomic locus and predicted protein isoforms, highlighting the mutation sites for the three mutant alleles and the protein domains of each isoform. All Ham protein isoforms maintain a functionally unknown motif PTZ00121 and the C-terminal zinc finger (ZF) clusters, while the long isoforms B/D and G also comprise the PR domain, the N-terminal ZF clusters. Isoform H has a truncated PR domain, and the shortest isoform E lacks the PR domain and the N-terminal ZF clusters. (**B**) Flanking sequences of the sgRNA target site from wt and four alleles with indels. Red letters indicate the sgRNA sequence. The corresponding amino acid sequence is shown above. "*" indicates the stop codon. (**C**). An image from western-blot, showing the two Ham protein bands in the control samples and absence of the Ham band(s) in the indicated mutants. "*" indicates an unspecific band, used as the loading control. (**D**) A table showing viability and sensory organ (SO) defects in four ham alleles. Note: the -6nt allele has a 6 nucleotide in-frame deletion. (**E**). Mechano-sensory organ phenotypes in the three indicated alleles. Red arrowheads indicate double sockets and double shafts phenotype.

Suppl._Figure 2. Ham expression and function in the female RS

(**A**). Bright-field images of the adult female RS from the indicated genotypes, showing accumulated eggs in the ham mutant ovaries. (**B**). Quantification of the number of progenies produced by wild-type and ham mutant females after crossed with wild-type males. Statistical significance was calculated using unpaired t-test (***, $p<0.001$; **, $p< 0.01$; *, $p<0.05$; ns, non-significant). (**C**). Images of pupal and adult ovaries and oviducts, showing high expression of the Ham_V5 protein in the connecting sites of the ovaries and oviducts.

Suppl._Figure 3. Split channel images for images in Fig. 2

Suppl._Figure 4. Ham controls the formation of TE epithelial cells

(A). Images of the testes from the early L3 larval stage, showing the absence of or mis-polarized TE terminal epithelial cell cluster in the *ham* mutant. E-Cad marks epithelial cells in green and DAPI marks the nuclei. The white arrows indicate mis-

polarized epithelial cells. (**B**). Illustration of the precursor cell clusters of the male RS in the embryonic stages. PGC, primordium germ cells; SGPs, somatic gonadal precursors; msSGP, male-specific SGPs. (**C-E**) Images of stage S13 and S15 *wt* embryos, showing Ham staining in all SGPs. Abd-B and Sox100B label msSGPs, VASA labels PGCs. (**F-G**). Images of the *wt* and *ham* mutant embryos at S13 (F) and S15 (G), showing the reduction or absence of msSGPs in the *hamSK1* mutant. Vasa is a germ cell marker, and Sox100B labels msSGPs in lime green.

Suppl._Figure 5. An epithelial-specific Gal4 line in the ham locus

(**A**). The *ham* gene locus, indicating the fragments in the Gal4 transgenes. The one (hamRSGal4) that drives reporter gene expression in the RS epithelial cells is highlighted in orange. (**B**). Images of pupal genital disc and TE in animals with hamRSGal4 and UAS-mCD8GFP. Ham_V5 is stained in magenta, and DAPI in blue. **(C).** Images showing the presence of myotubes on the surface of the testis. The bar graph on the right shows the relative abundance of myotubes on the testis in wt (100%) and ham mutant condition quantified from five animals each. **(D).** Images showing the junction between the TE and SV, and myotubes are present even in the *ham* mutant. The white arrows indicate myotubes with two or three nuclei at the junction.

Suppl._Figure 6. Ham regulatory activity and potential co-factors

(**A**). Principle component analysis of the RNA-seq datasets. **(B)**. Principle component analysis of the Cut&Tag datasets. Note: some samples had poor sequencing depth, which were excluded from the PCA and later analyses. **(C)**. The *shot* locus, showing the CUT&TAG tracks from the TE and GD (TG) mixed samples and the enhancer fragments in the luciferase assays. (**D**). Normalized luciferase activity to the empty reporter and then to the control vector that expresses GFP and RFP proteins. Statistical significance was calculated using unpaired t-test (****, $p<0.0001$; ***, $p<0.001$; **, $p< 0.01$; *, $p<0.05$; ns, non-significant). (**E**). Significantly enriched motifs from Ham binding peaks in up-regulated genes (left) and downregulated genes (right). The dashed rectangles highlight MAD and ZNF263 motifs.

Suppl._Figure 7. Split channel images for images in Fig. 5

Suppl._Figure 8. Split channel images for images in Fig. 5

Suppl._Figure 9. Expression of genes tested by SCRINSHOT in RNA-seq data

(A) Log2FC (hamSK1/Df versus wt/Df and *hamPRΔ* versus wt) in TE. **(B)** Log2FC(hamSK1/Df versus wt/Df and *hamPRΔ* versus wt) in GD.

Suppl._Figure 10. Split channel images for images in Fig. 6

Suppl._Figure 11. Additional genes tested in SCRINSHOT

(**A**). Images from SCRINSHOT, showing mRNA signal of the indicated genes in *wt* TE samples. DNA is marked by DAPI in grey. (**B**). Images from SCRINSHOT, showing mRNA signal of the indicated genes in *wt* TE samples at a later pupal stage (28-32 APF). DNA is marked by DAPI in grey. (**C**). Images from SCRINSHOT, showing mRNA signals of indicated genes in *wt/Df* and *hamSK1/Df* mutant GDs. (**D**). Images from SCRINSHOT, showing mRNA signals of indicated genes in *GFP* and *ham RNAi* GD samples. (**E-F**). Quantification of signal intensity for genes shown in C-D in two areas, the SV and EjD. (**G**). Quantification of signal intensity for genes that changed expression in ham RNAi TE. Statistical significance was calculated using unpaired t-test (***, $p<0.001$; **, $p< 0.01$; *, $p<0.05$; ns, non-significant).

Suppl._Figure 12-13. Split channel images for images in Suppl._Figure 11

Suppl._Figure 14. Male fertility test for Toll-9

(**A**). Graphs of progeny number from male fertility test for hamRSGal4 driving *Toll-9* RNAi in comparison to GFP RNAi. The number of tested males =3. (**B**). White-field image of Toll-9 RNAi adult male RS, showing morphological defects of the TE and the phenotype penetrance (11% of 37 animals). (**C**). Images of adult RS from control GFP RNAi andToll-9 RNAi males. hamRSGal4>UAS-mCD8GFP is used to label the testis terminal epithelium and the SV, and DAPI stains DNA. The panels below are higher magnification views on the selected SV area, highlighted with white dashed squares. White arrows indicate sperms in the control SV, which are absent from the Toll-RNAi sample. The bar graph shows the percentage of SV with sperms in GFP and Toll-9 RNAi animals (N=10).

Suppl._Figure 15. PRDM16 and MECOM/PRDM3 expression in human tissues

(A). RNA expression data across human tissues through Cap analysis of gene expression (Fantom5 dataset from the Human Protein Atlas). **(B).** Expression in Single cell RNA-seq clusters in the indicated human tissues (from the Human Protein Atlas).

A

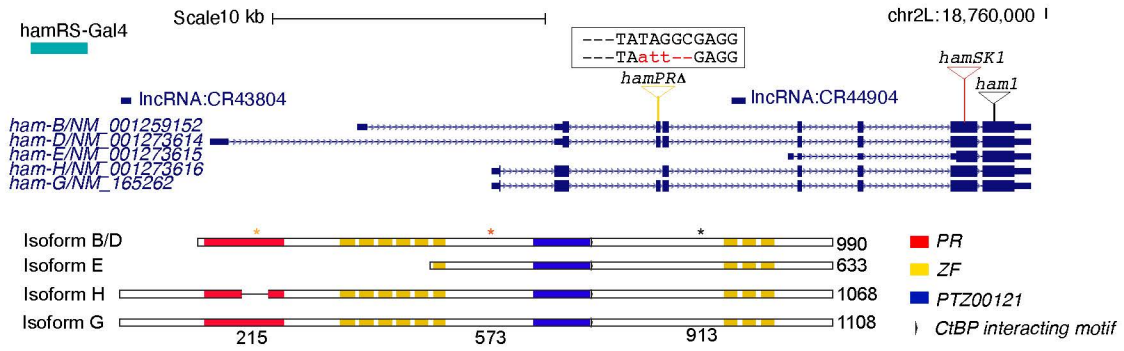

B

```
     I  R  S  V  Q  D  D  C  I  G  E  A  N  L  Q  S
  wt ATCCGAAGCGTTCAGGACGATTGTATAGGCGAGGCTAATTTACAGAGT

     I  R  S  V  Q  D  D  C  N  *
-5+3 ATCCGAAGCGTTCAGGACGATTGTAATT--GAGGCTAATTTACAGAGT

     I  R  S  V  Q  D  D  C  I  G        *
  -5 ATCCGAAGCGTTCAGGACGATTGTATAGGC-----TAATTTACAGAGT

     I  R  S  V  Q  A                R  L  I  Y  R
 -13 ATCCGAAGCGTTCAGG-------------CGAGGCTAATTTACAGAGT

     I  R  S  V  Q  D  D  T         E  A  N  L  Q  S
  -6 ATCCGAAGCGTTCAGGACGATT------GCGAGGCTAATTTACAGAGT
```

C

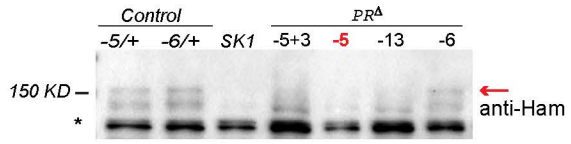

D

ham	Trans-heterozygous ham/ham Df	
	Lethality	SO defects
-5nts	semi-lethal (60.6% survival)	0
-6nts	Viable (100% survival)	0
ham[1]	die upon hatch	100%
ham[sk1]	die upon hatch	100%

E

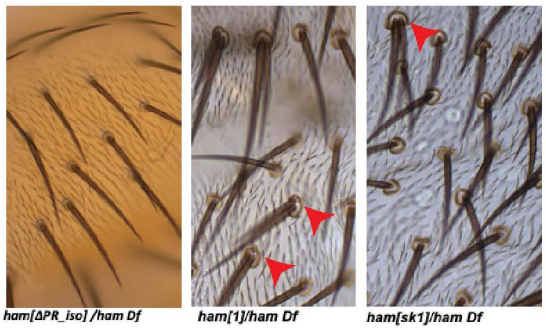

A

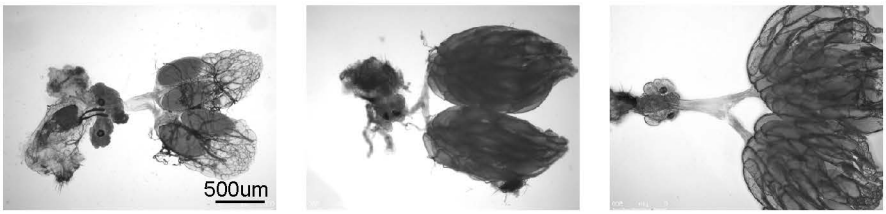

wt hamPRΔ/hamPRΔ hamPRΔ/Df

B

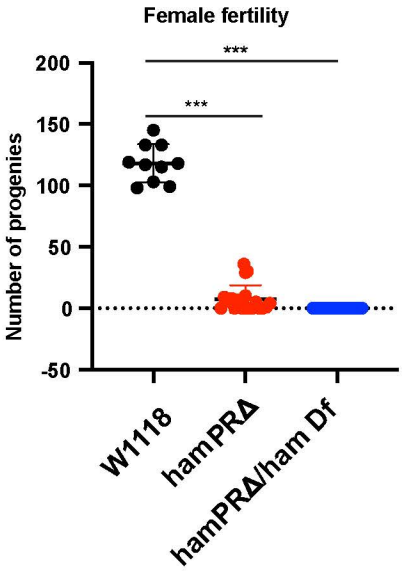

C

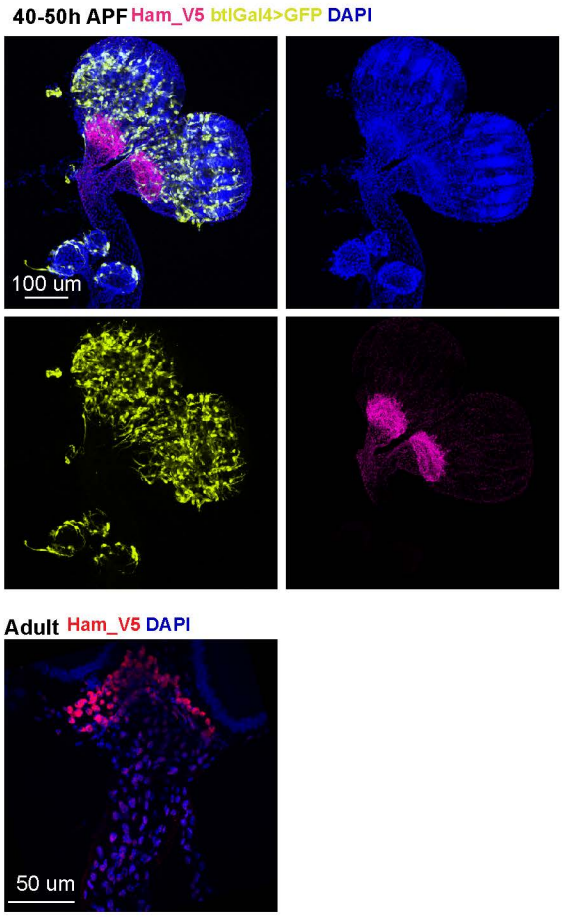

A Fig2B split channels

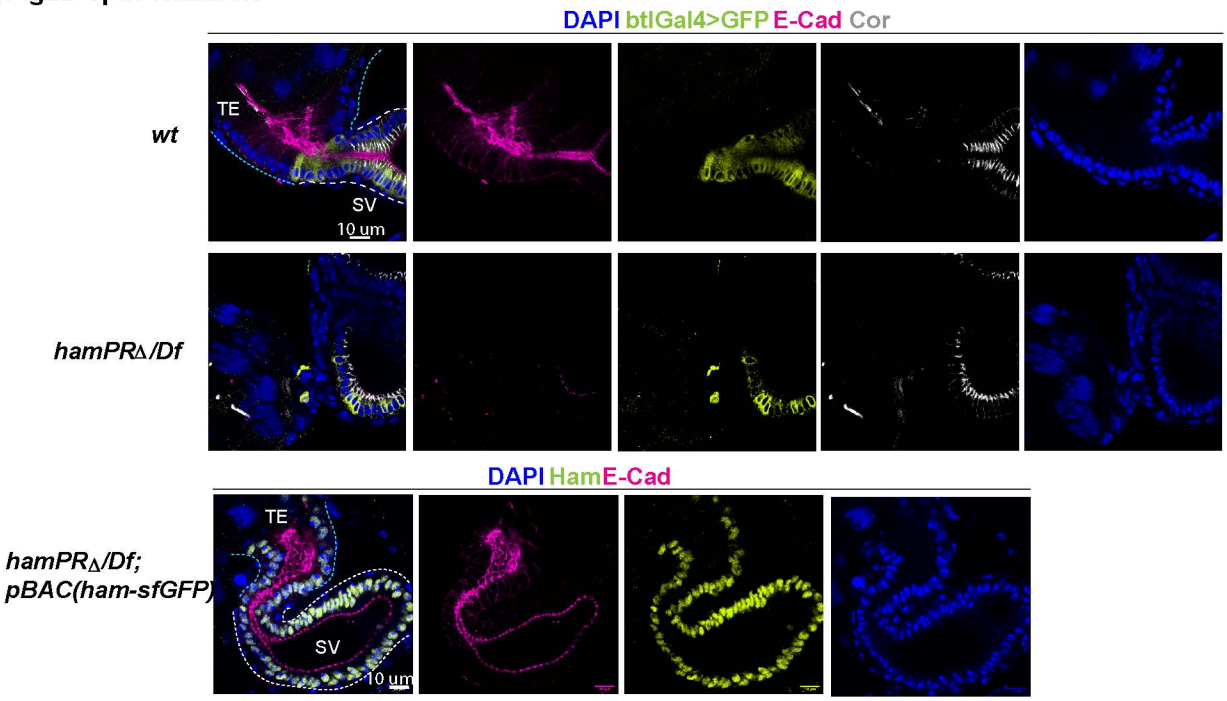

B Fig2F split channels

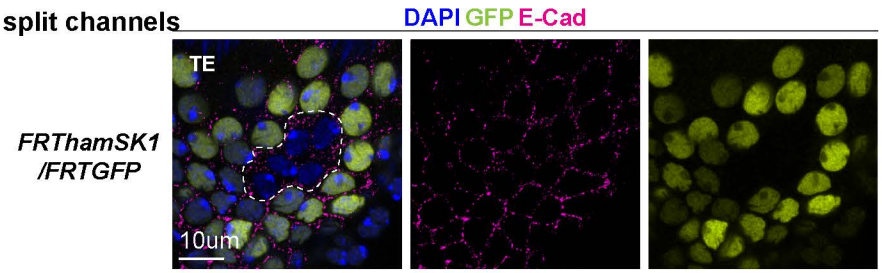

C Fig2I split channels

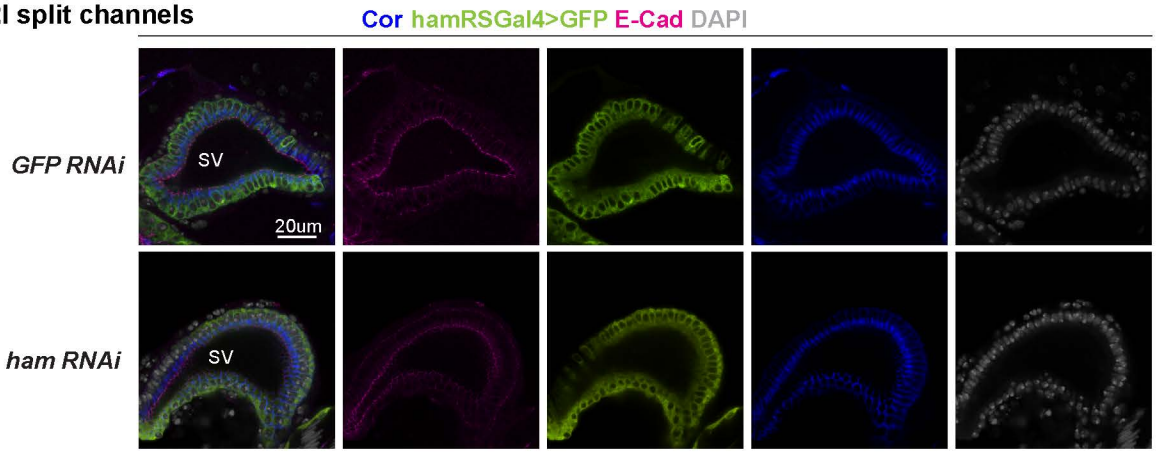

D Fig2J split channels

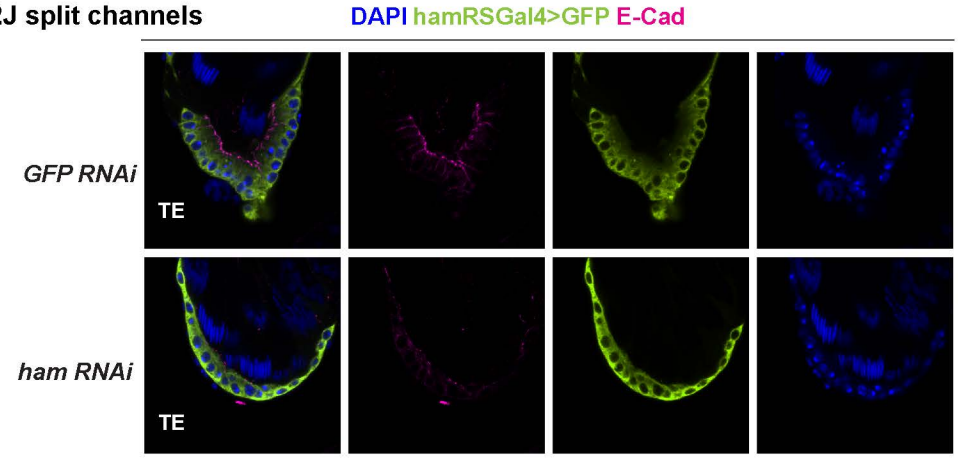

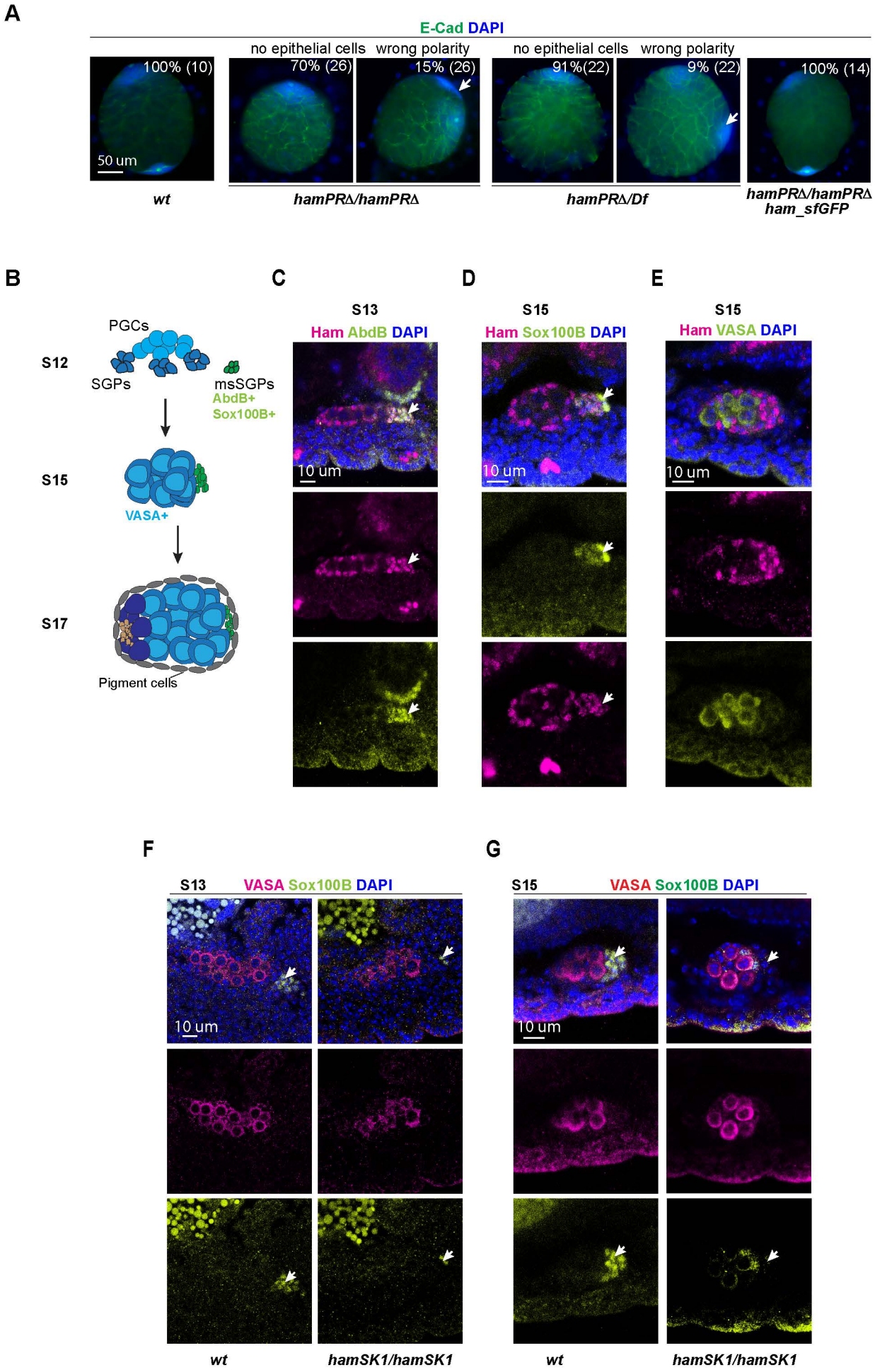
A
E-Cad DAPI
no epithelial cells
wrong polarity
no epithelial cells
wrong polarity
100% (10)
70% (26)
15% (26)
91%(22)
9% (22)
100% (14)
50 um
wt
hamPRΔ/hamPRΔ
hamPRΔ/Df
hamPRΔ/hamPRΔ
ham_sfGFP
B
PGCs
S12
SGPs
msSGPs
AbdB+
Sox100B+
S15
VASA+
S17
Pigment cells
C
S13
Ham AbdB DAPI
10 um
D
S15
Ham Sox100B DAPI
10 um
E
S15
Ham VASA DAPI
10 um
F
S13
VASA Sox100B DAPI
10 um
wt
hamSK1/hamSK1
G
S15
VASA Sox100B DAPI
10 um
wt
hamSK1/hamSK1

A

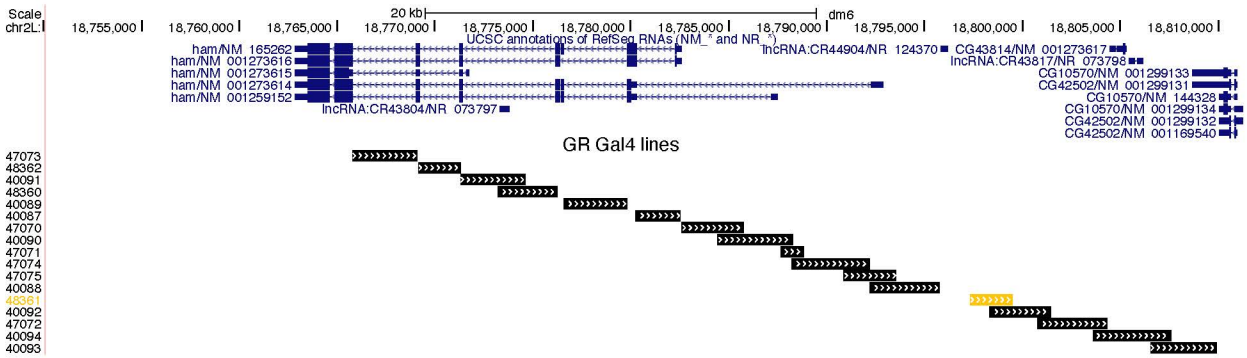

B

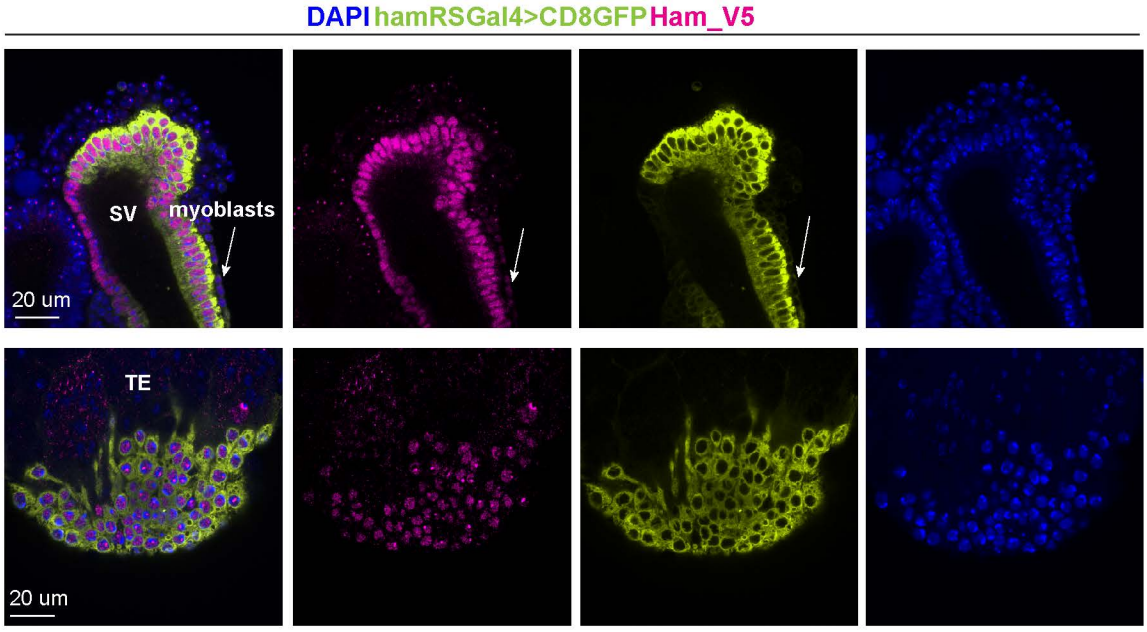

C

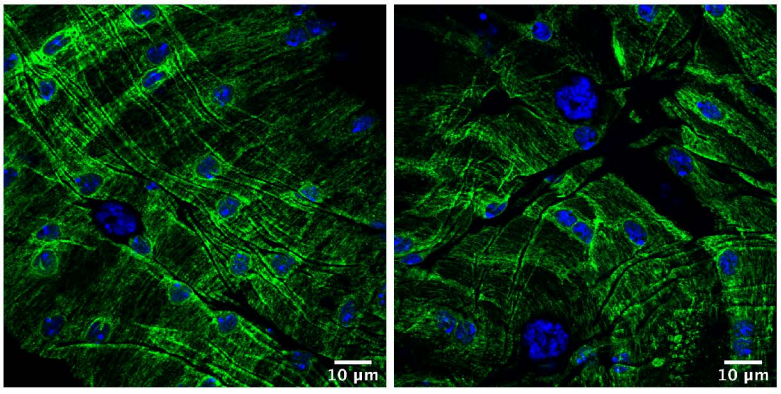

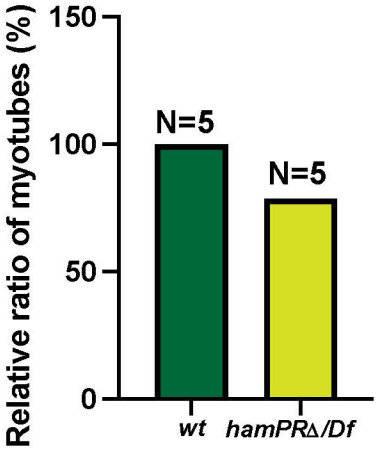

D

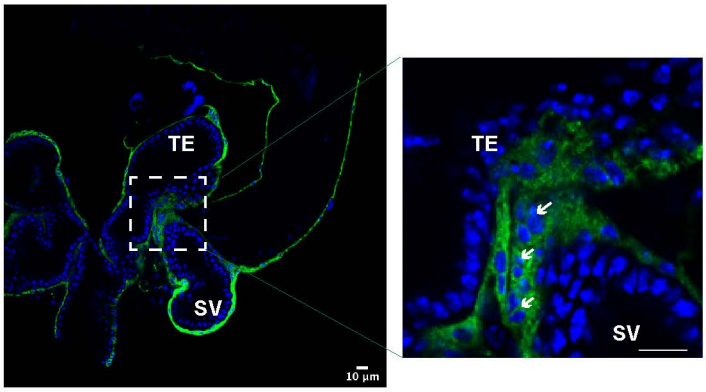

hamPRΔ/Df

A

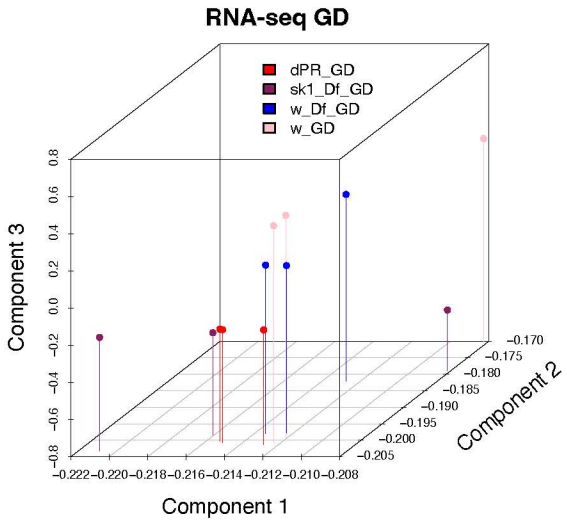
RNA-seq GD
dPR_GD
sk1_Df_GD
w_Df_GD
w_GD
Component 1
Component 2
Component 3

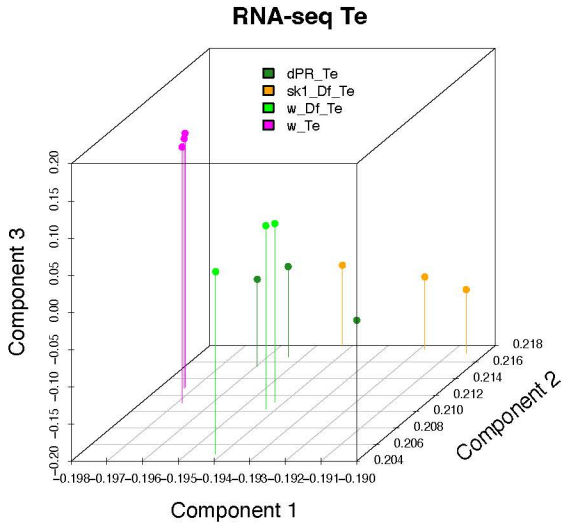
RNA-seq Te
dPR_Te
sk1_Df_Te
w_Df_Te
w_Te
Component 1
Component 2
Component 3

B

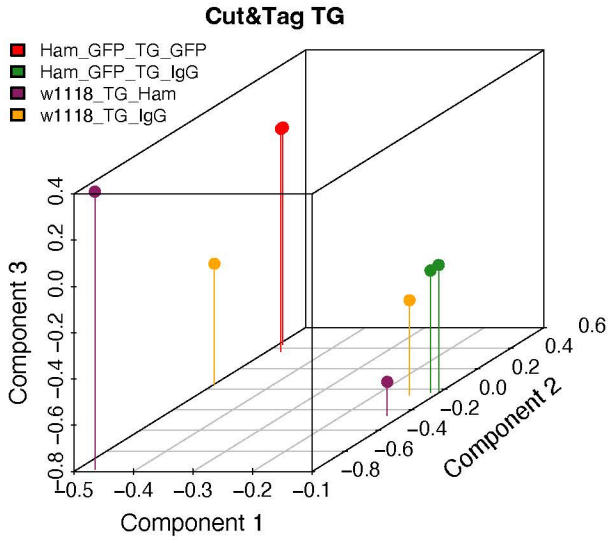
Cut&Tag TG
Ham_GFP_TG_GFP
Ham_GFP_TG_IgG
w1118_TG_Ham
w1118_TG_IgG
Component 1
Component 2
Component 3

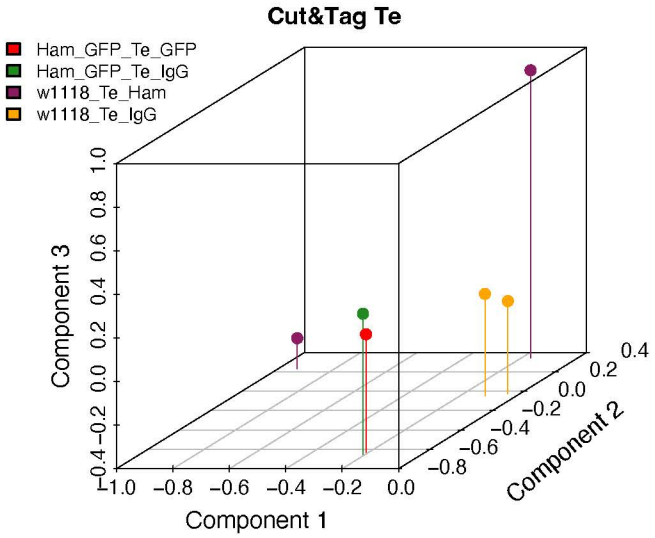
Cut&Tag Te
Ham_GFP_Te_GFP
Ham_GFP_Te_IgG
w1118_Te_Ham
w1118_Te_IgG
Component 1
Component 2
Component 3

C

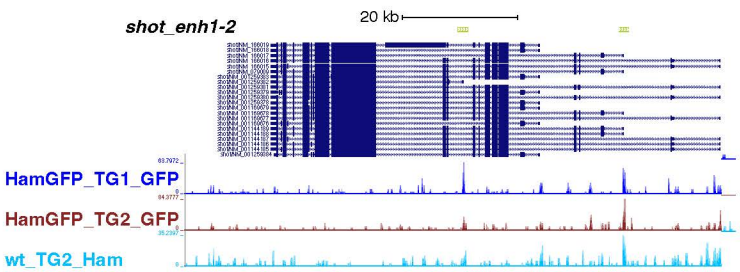
shot_enh1-2
20 kb
HamGFP_TG1_GFP
HamGFP_TG2_GFP
wt_TG2_Ham

D

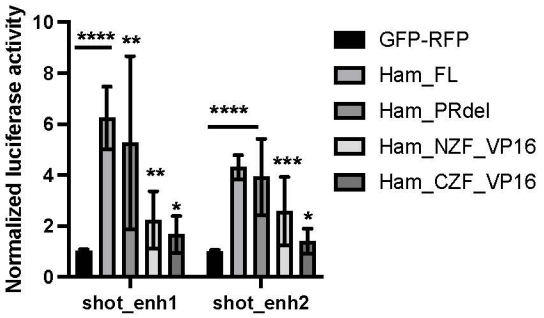
Normalized luciferase activity
GFP-RFP
Ham_FL
Ham_PRdel
Ham_NZF_VP16
Ham_CZF_VP16
shot_enh1
shot_enh2

E

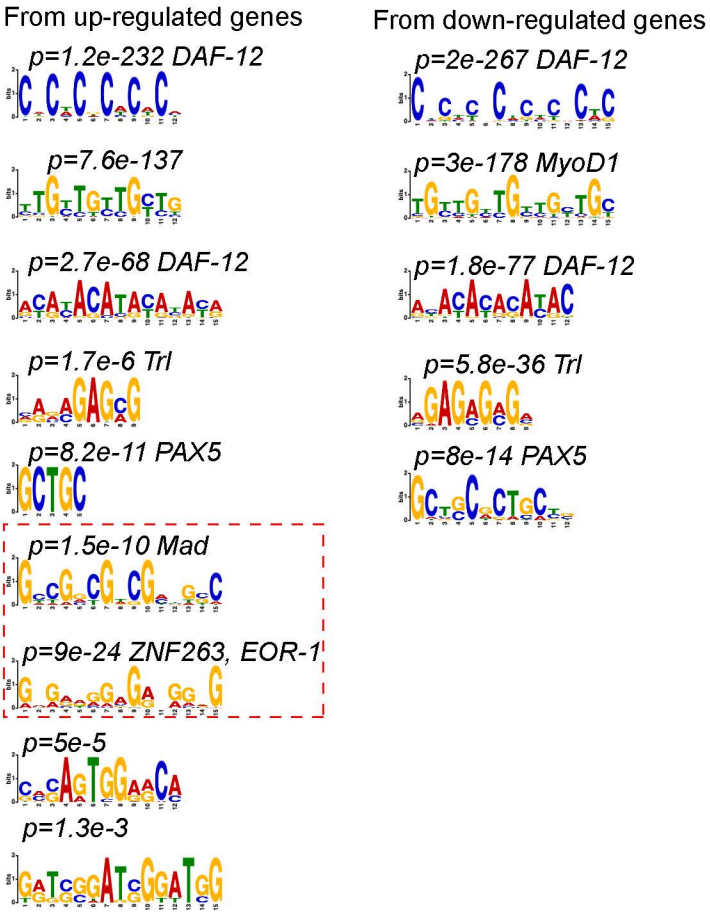
From up-regulated genes
From down-regulated genes
p=1.2e-232 DAF-12
p=7.6e-137
p=2.7e-68 DAF-12
p=1.7e-6 Trl
p=8.2e-11 PAX5
p=1.5e-10 Mad
p=9e-24 ZNF263, EOR-1
p=5e-5
p=1.3e-3
p=2e-267 DAF-12
p=3e-178 MyoD1
p=1.8e-77 DAF-12
p=5.8e-36 Trl
p=8e-14 PAX5

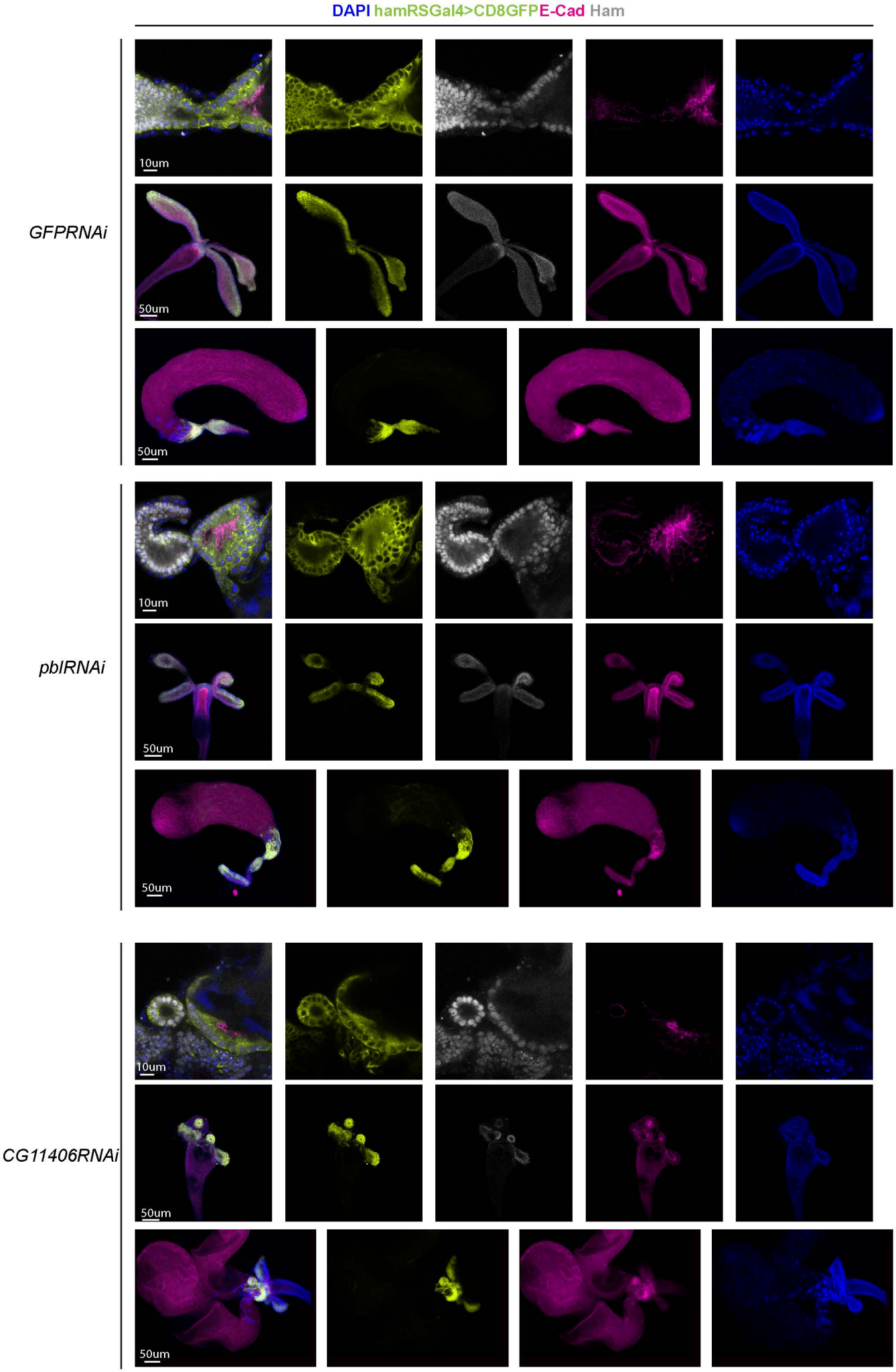
DAPI hamRSGal4>CD8GFPE-Cad Ham
GFPRNAi
pblRNAi
CG11406RNAi
10um
50um

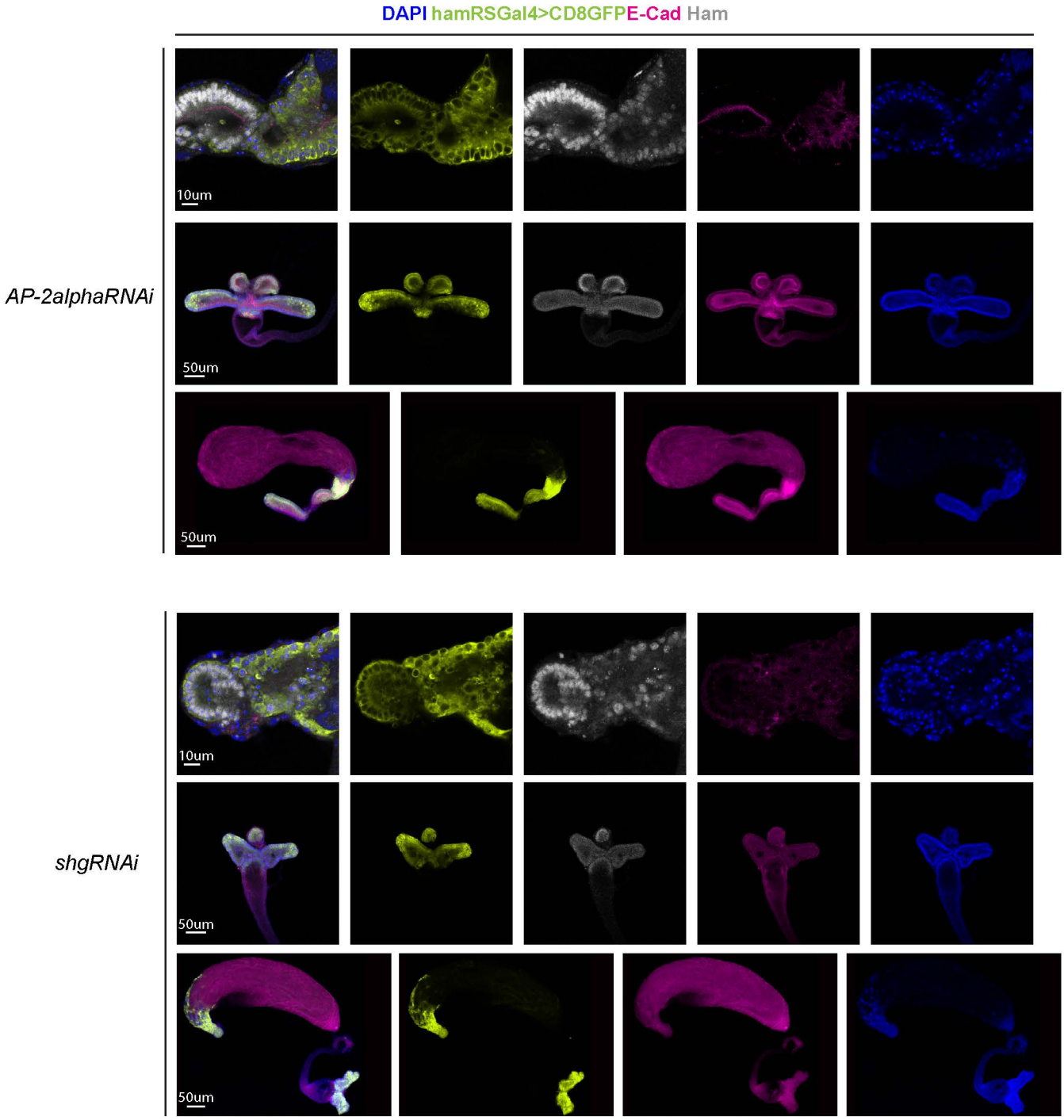
DAPI hamRSGal4>CD8GFPE-Cad Ham
AP-2alphaRNAi
10um
50um
50um
shgRNAi
10um
50um
50um

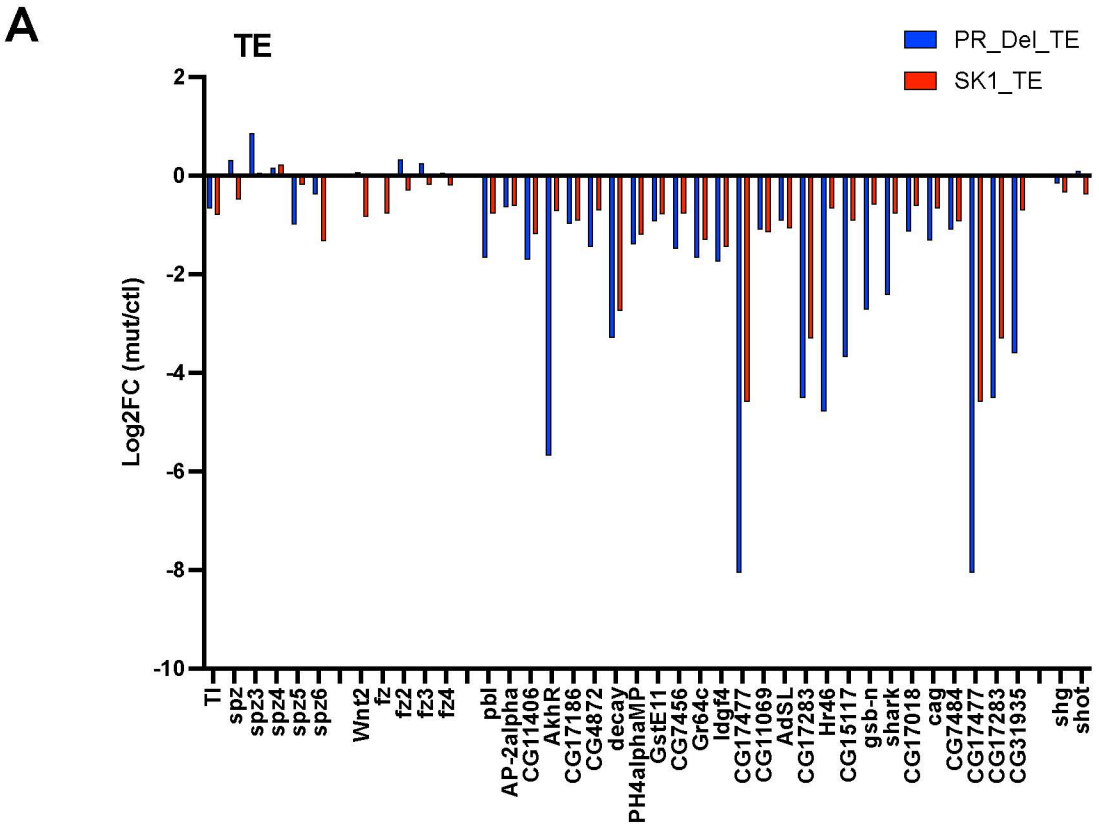
A
TE
PR_Del_TE
SK1_TE
Log2FC (mut/ctl)
2
0
-2
-4
-6
-8
-10
Tl
spz
spz3
spz4
spz5
spz6
Wnt2
fz
fz2
fz3
fz4
pbl
AP-2alpha
CG11406
AkhR
CG17186
CG4872
decay
PH4alphaMP
GstE11
CG7456
Gr64c
ldgf4
CG17477
CG11069
AdSL
CG17283
Hr46
CG15117
gsb-n
shark
CG17018
cag
CG7484
CG17477
CG17283
CG31935
shg
shot

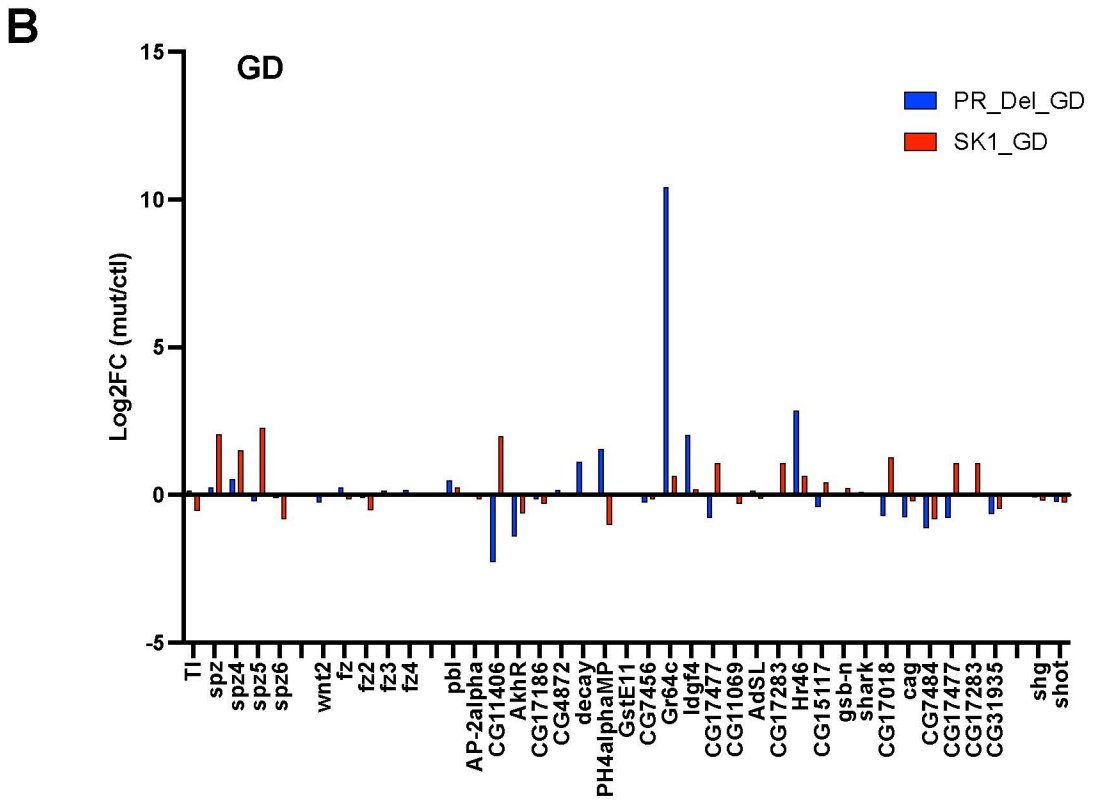
B
GD
PR_Del_GD
SK1_GD
Log2FC (mut/ctl)
15
10
5
0
-5
Tl
spz
spz4
spz5
spz6
wnt2
fz
fz2
fz3
fz4
pbl
AP-2alpha
CG11406
AkhR
CG17186
CG4872
decay
PH4alphaMP
GstE11
CG7456
Gr64c
ldgf4
CG17477
CG11069
AdSL
CG17283
Hr46
CG15117
gsb-n
shark
CG17018
cag
CG7484
CG17477
CG17283
CG31935
shg
shot

A Fig6A split channels

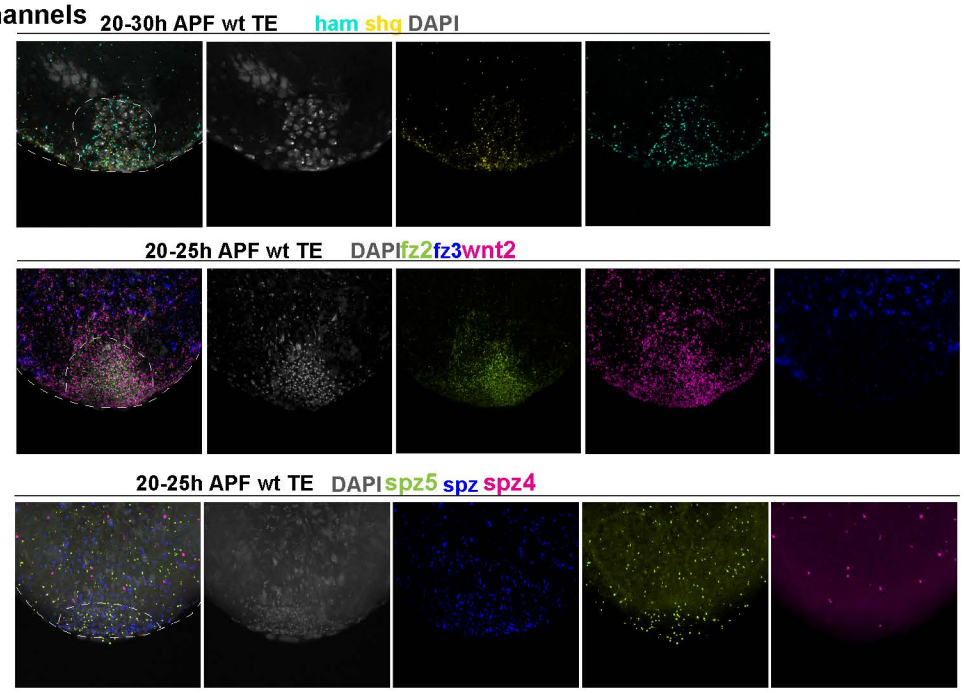

B Fig6B split channels

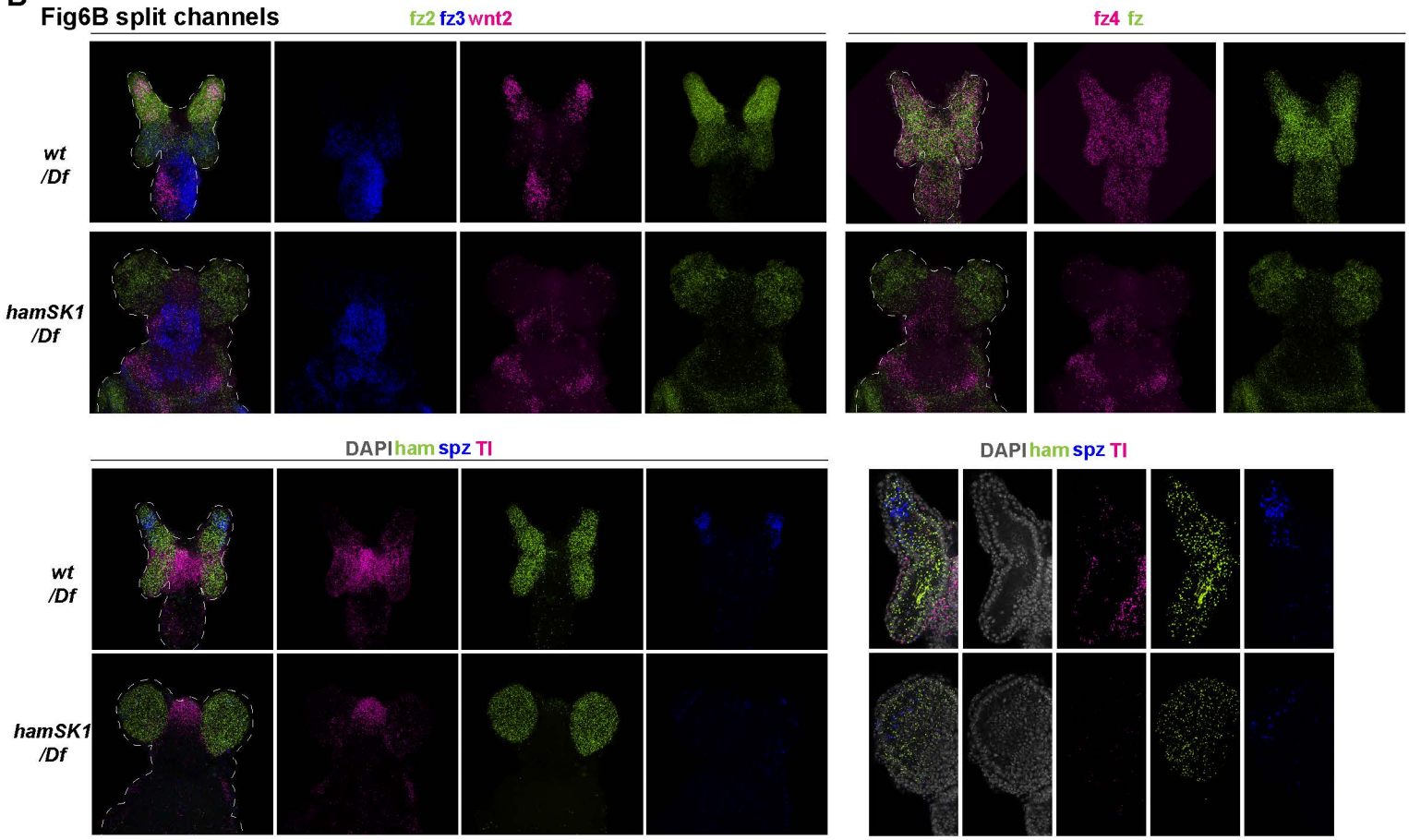

C Fig6D split channels

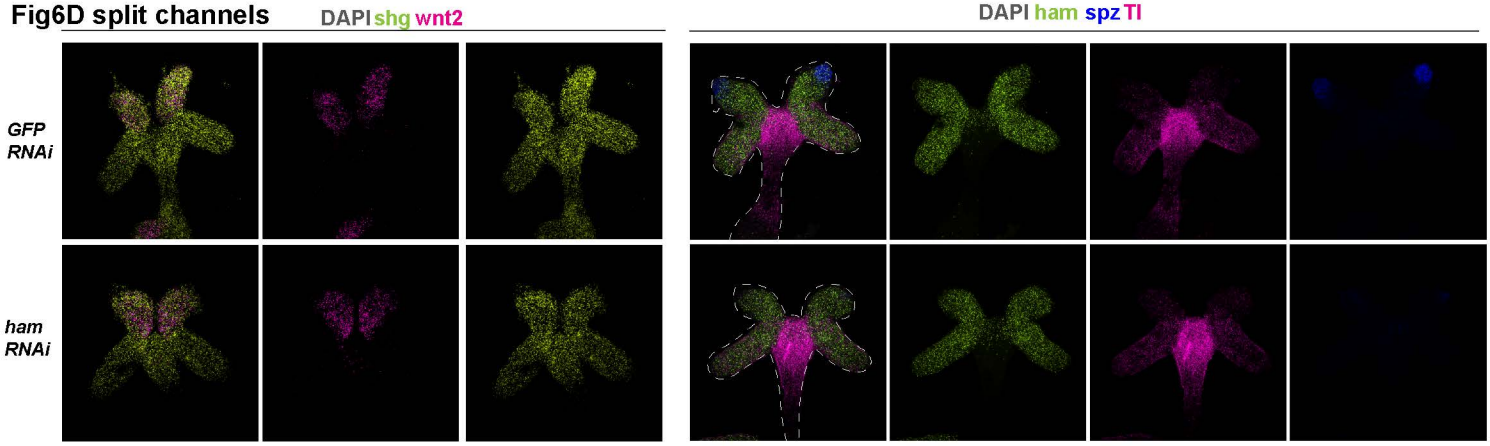

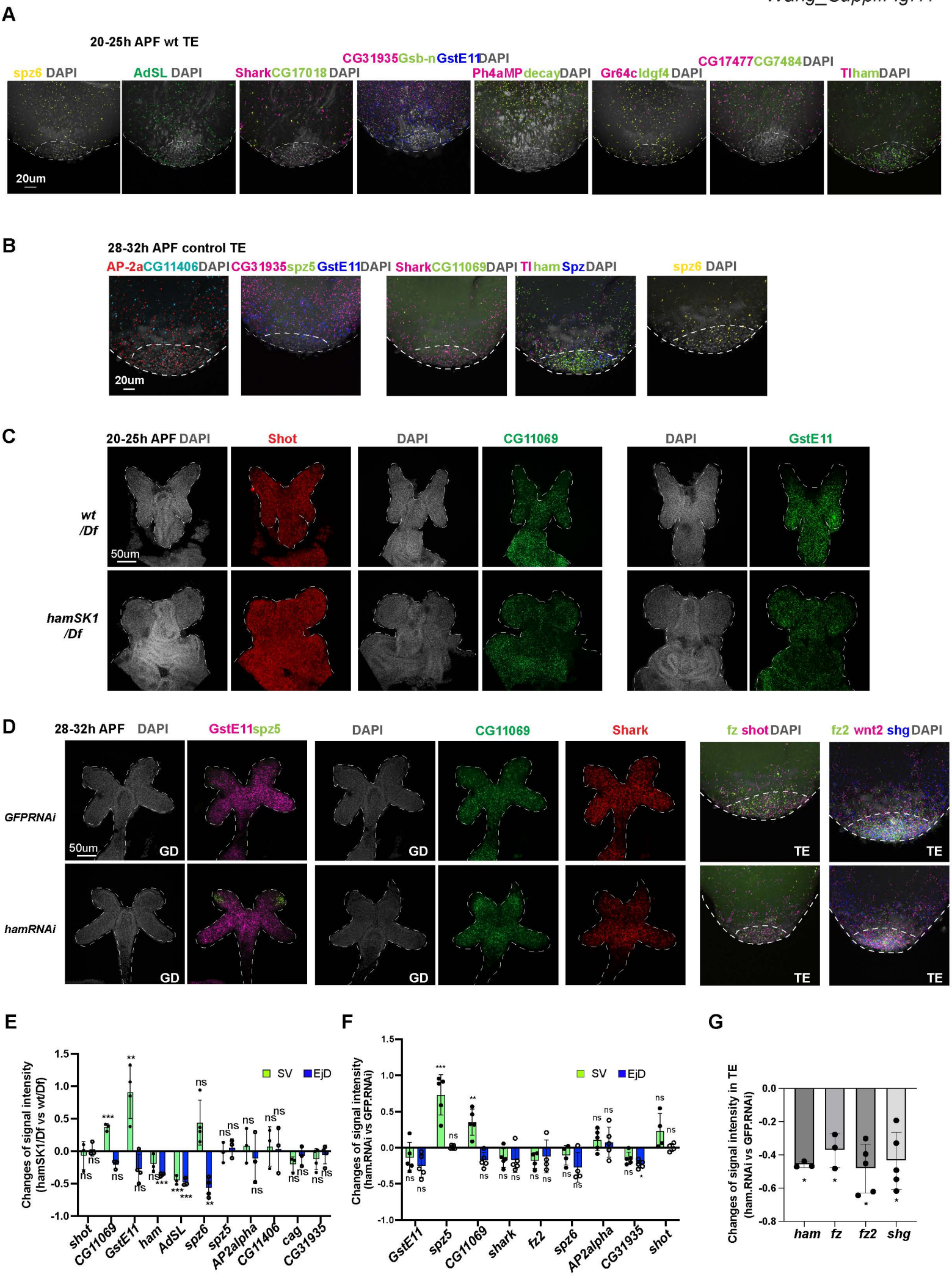
A
20-25h APF wt TE
spz6 DAPI
AdSL DAPI
SharkCG17018 DAPI
CG31935Gsb-nGstE11DAPI
Ph4aMPdecayDAPI
Gr64cIdgf4 DAPI
CG17477CG7484DAPI
TlhamDAPI
20um
B
28-32h APF control TE
AP-2aCG11406DAPI
CG31935spz5GstE11DAPI
SharkCG11069DAPI
TlhamSpzDAPI
spz6 DAPI
20um
C
20-25h APF DAPI
Shot
DAPI
CG11069
DAPI
GstE11
wt /Df
hamSK1 /Df
50um
D
28-32h APF DAPI
GstE11spz5
DAPI
CG11069
Shark
fz shot DAPI
fz2 wnt2 shg DAPI
GFPRNAi
hamRNAi
50um
GD
TE
E
Changes of signal intensity (hamSK1/Df vs wt/Df)
SV
EjD
shot
CG11069
GstE11
ham
AdSL
spz6
spz5
AP2alpha
CG11406
cag
CG31935
F
Changes of signal intensity (ham.RNAi vs GFP.RNAi)
SV
EjD
GstE11
spz5
CG11069
shark
fz2
spz6
AP2alpha
CG31935
shot
G
Changes of signal intensity in TE (ham.RNAi vs GFP.RNAi)
ham
fz
fz2
shg

Supplementary Fig. 11A split channels

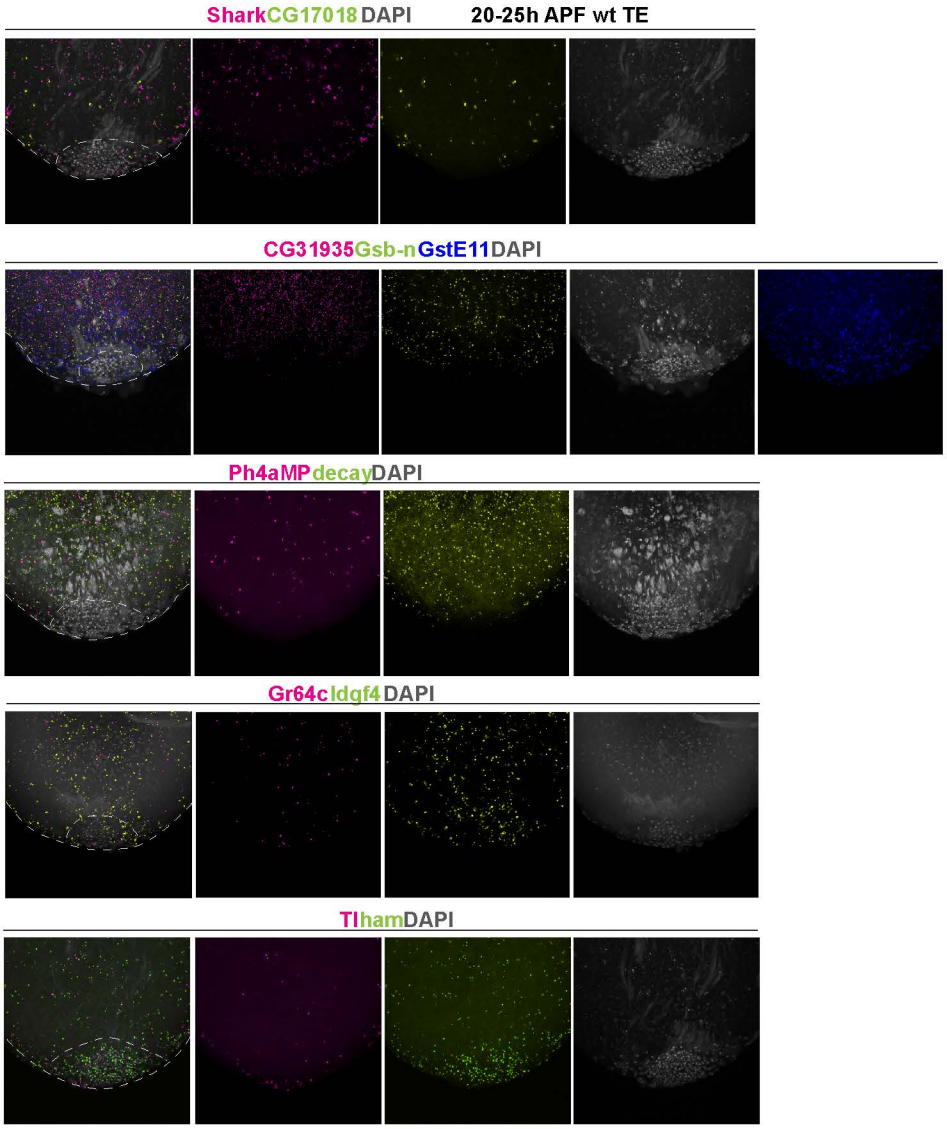

Supplementary Fig. 11B split channels

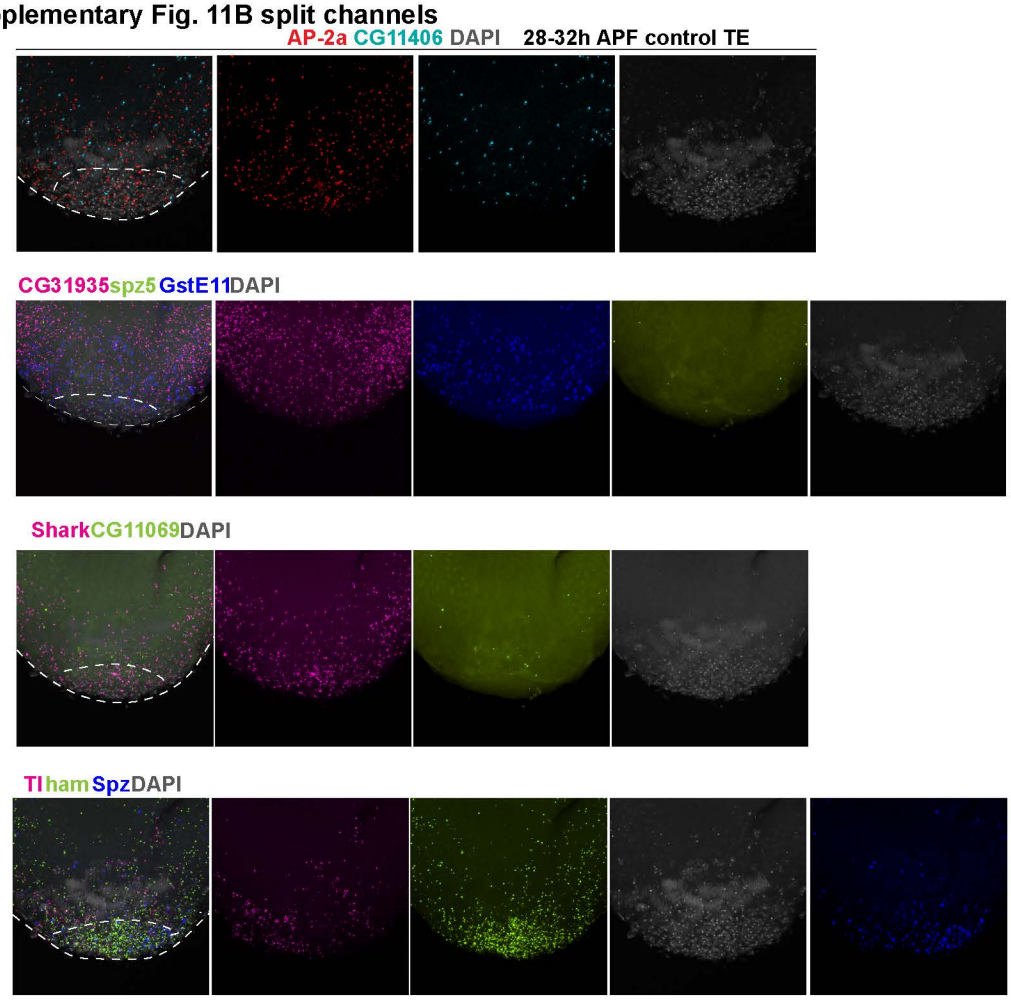

Supplementary Fig. 11D split channels

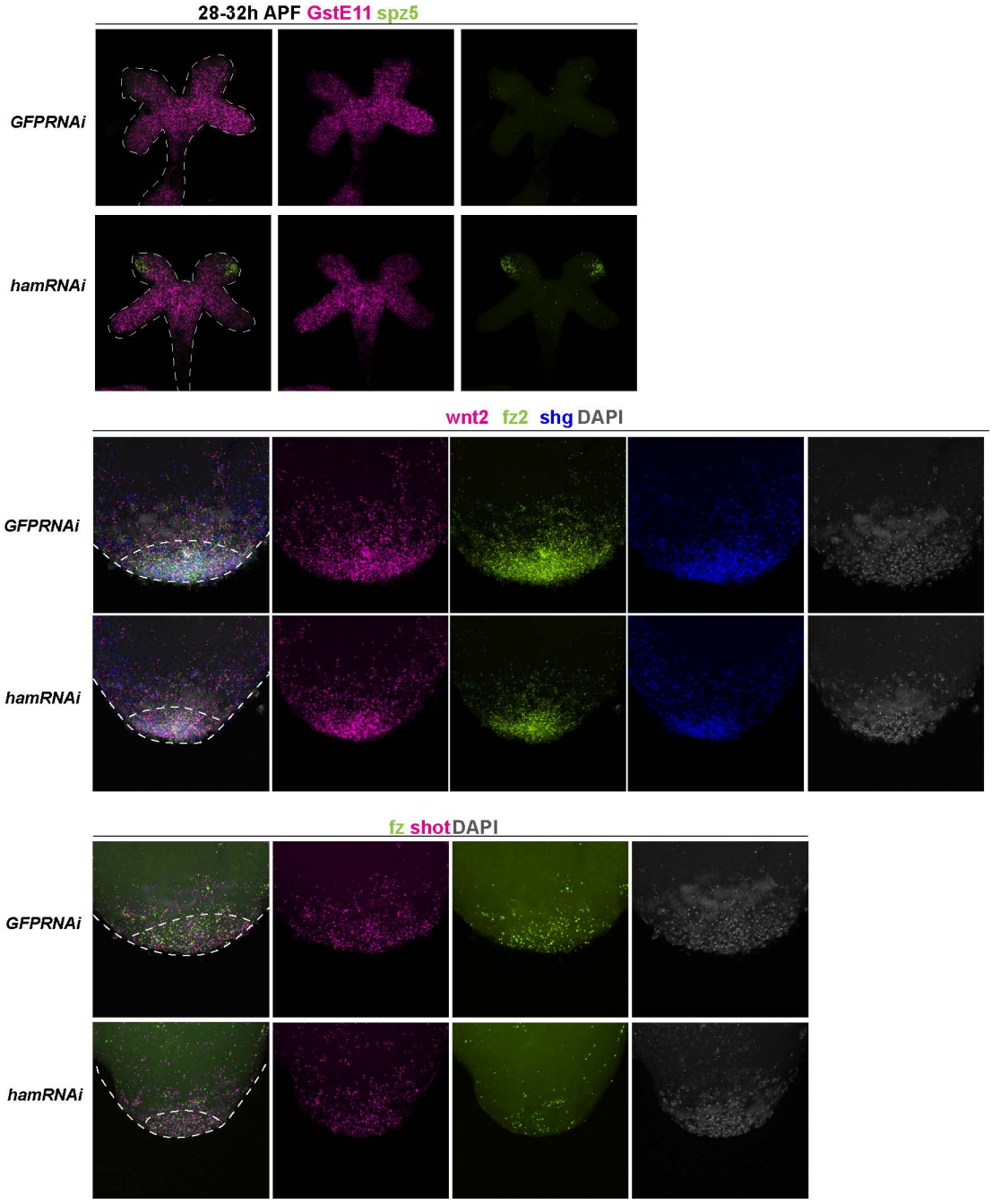

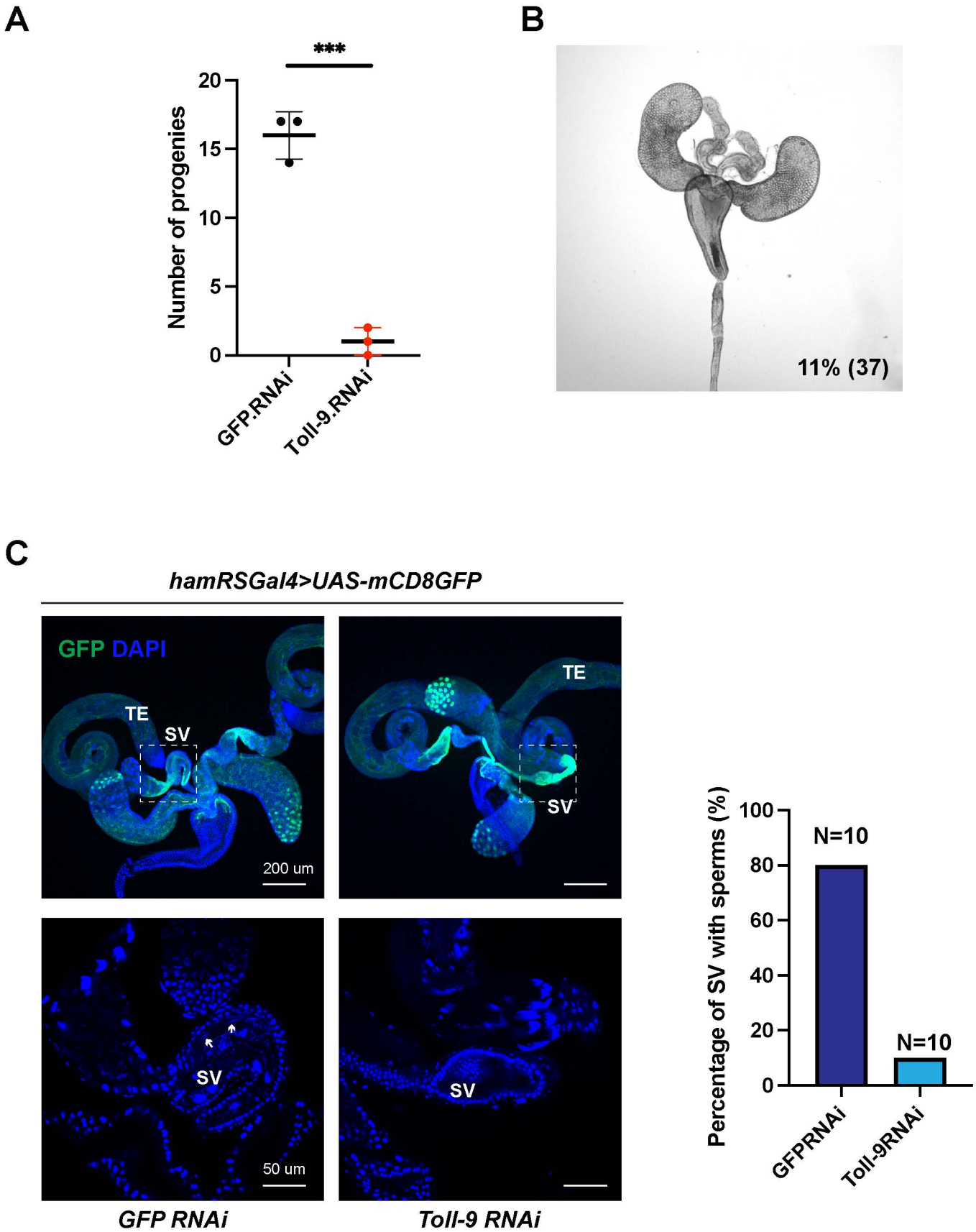
A
***
Number of progenies
20
15
10
5
0
GFP.RNAi
Toll-9.RNAi
B
11% (37)
C
hamRSGal4>UAS-mCD8GFP
GFP DAPI
TE
SV
200 um
TE
SV
SV
50 um
SV
GFP RNAi
Toll-9 RNAi
Percentage of SV with sperms (%)
100
80
60
40
20
0
N=10
N=10
GFPRNAi
Toll-9RNAi

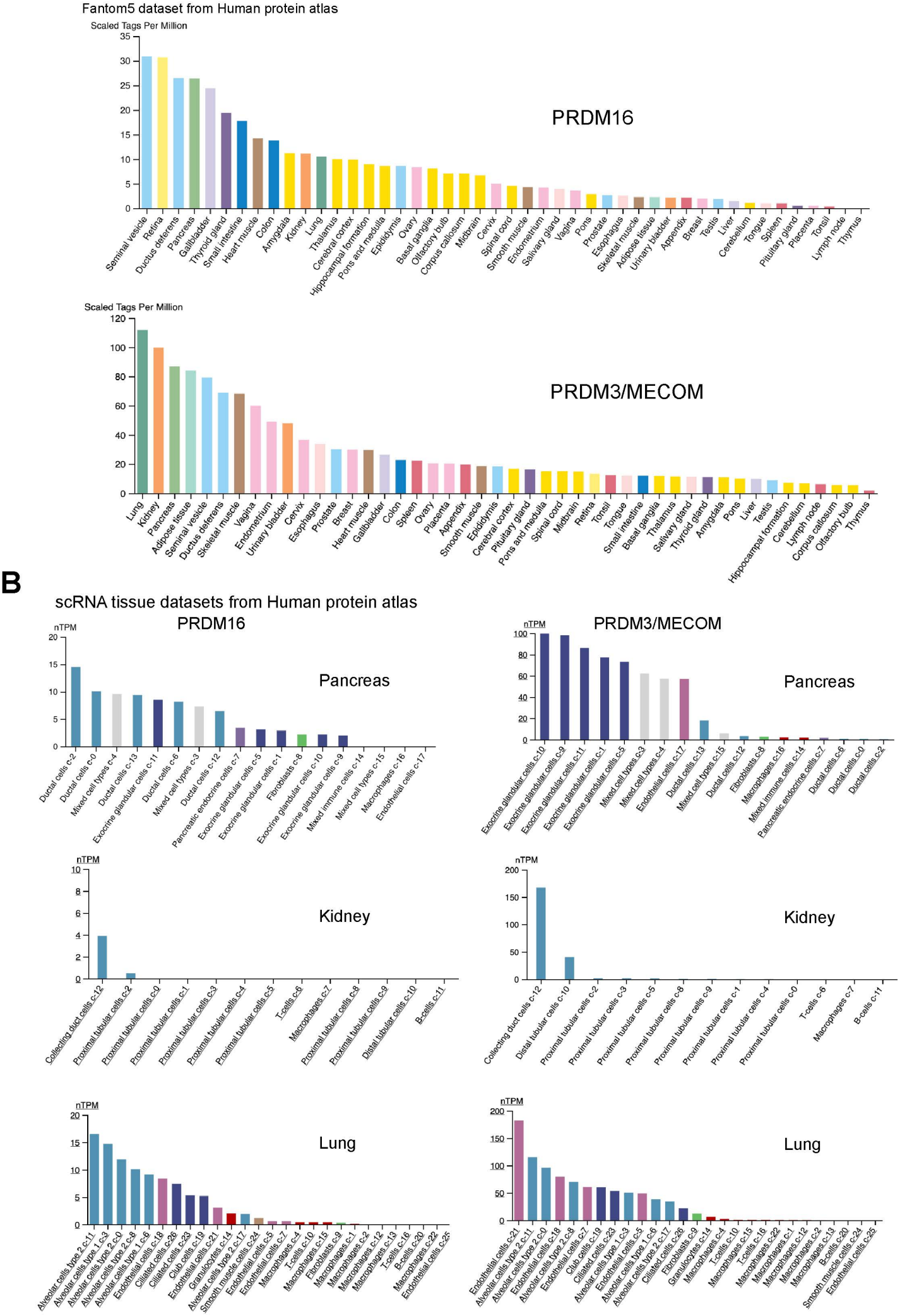
A
Fantom5 dataset from Human protein atlas
Scaled Tags Per Million
PRDM16
Seminal vesicle
Retina
Ductus deferens
Pancreas
Gallbladder
Thyroid gland
Small intestine
Heart muscle
Colon
Amygdala
Kidney
Lung
Thalamus
Cerebral cortex
Hippocampal formation
Pons and medulla
Epididymis
Ovary
Basal ganglia
Olfactory bulb
Corpus callosum
Midbrain
Cervix
Spinal cord
Smooth muscle
Endometrium
Salivary gland
Vagina
Pons
Prostate
Esophagus
Skeletal muscle
Adipose tissue
Urinary bladder
Appendix
Breast
Testis
Liver
Cerebellum
Tongue
Spleen
Pituitary gland
Placenta
Tonsil
Lymph node
Thymus
Scaled Tags Per Million
PRDM3/MECOM
Lung
Kidney
Pancreas
Adipose tissue
Seminal vesicle
Ductus deferens
Skeletal muscle
Vagina
Endometrium
Urinary bladder
Cervix
Esophagus
Prostate
Breast
Heart muscle
Gallbladder
Colon
Spleen
Ovary
Placenta
Appendix
Smooth muscle
Epididymis
Cerebral cortex
Pituitary gland
Pons and medulla
Spinal cord
Midbrain
Retina
Tonsil
Tongue
Small intestine
Basal ganglia
Thalamus
Salivary gland
Thyroid gland
Amygdala
Pons
Liver
Testis
Hippocampal formation
Cerebellum
Lymph node
Corpus callosum
Olfactory bulb
Thymus
B
scRNA tissue datasets from Human protein atlas
PRDM16
nTPM
Pancreas
Ductal cells c-2
Ductal cells c-0
Mixed cell types c-4
Ductal cells c-13
Exocrine glandular cells c-11
Ductal cells c-6
Mixed cell types c-3
Ductal cells c-12
Pancreatic endocrine cells c-7
Exocrine glandular cells c-5
Exocrine glandular cells c-1
Fibroblasts c-8
Exocrine glandular cells c-10
Exocrine glandular cells c-9
Mixed immune cells c-14
Mixed cell types c-15
Macrophages c-16
Endothelial cells c-17
PRDM3/MECOM
nTPM
Pancreas
Exocrine glandular cells c-10
Exocrine glandular cells c-9
Exocrine glandular cells c-11
Exocrine glandular cells c-1
Exocrine glandular cells c-5
Mixed cell types c-3
Mixed cell types c-4
Endothelial cells c-17
Ductal cells c-13
Mixed cell types c-15
Ductal cells c-12
Fibroblasts c-8
Macrophages c-16
Mixed immune cells c-14
Pancreatic endocrine cells c-7
Ductal cells c-6
Ductal cells c-0
Ductal cells c-2
nTPM
Kidney
Collecting duct cells c-12
Proximal tubular cells c-2
Proximal tubular cells c-0
Proximal tubular cells c-1
Proximal tubular cells c-3
Proximal tubular cells c-4
Proximal tubular cells c-5
T-cells c-6
Macrophages c-7
Proximal tubular cells c-8
Proximal tubular cells c-9
Proximal tubular cells c-10
B-cells c-11
nTPM
Kidney
Collecting duct cells c-12
Distal tubular cells c-10
Proximal tubular cells c-2
Proximal tubular cells c-3
Proximal tubular cells c-5
Proximal tubular cells c-8
Proximal tubular cells c-9
Proximal tubular cells c-1
Proximal tubular cells c-4
Proximal tubular cells c-0
T-cells c-6
Macrophages c-7
B-cells c-11
nTPM
Lung
Alveolar cells type 2 c-11
Alveolar cells type 1 c-3
Alveolar cells type 2 c-0
Alveolar cells type 2 c-8
Alveolar cells type 1 c-6
Endothelial cells c-18
Ciliated cells c-26
Ciliated cells c-23
Club cells c-19
Endothelial cells c-21
Granulocytes c-14
Alveolar cells type 2 c-17
Smooth muscle cells c-24
Endothelial cells c-5
Endothelial cells c-7
Macrophages c-4
T-cells c-10
Macrophages c-15
Fibroblasts c-9
Macrophages c-1
Macrophages c-2
Macrophages c-12
Macrophages c-13
T-cells c-16
B-cells c-20
Macrophages c-22
Endothelial cells c-25
nTPM
Lung
Endothelial cells c-21
Alveolar cells type 2 c-11
Alveolar cells type 2 c-0
Endothelial cells c-18
Alveolar cells type 2 c-8
Endothelial cells c-7
Club cells c-19
Ciliated cells c-23
Alveolar cells type 1 c-3
Endothelial cells c-5
Alveolar cells type 1 c-6
Alveolar cells type 2 c-17
Ciliated cells c-26
Fibroblasts c-9
Granulocytes c-14
Macrophages c-4
T-cells c-10
Macrophages c-15
T-cells c-16
Macrophages c-22
Macrophages c-1
Macrophages c-12
Macrophages c-2
Macrophages c-13
B-cells c-20
Smooth muscle cells c-24
Endothelial cells c-25